Circuit quantum electrodynamic model of dissipative-dispersive Josephson traveling-wave parametric amplifiers

Yongjie Yuan,[1] Michael Haider,[1,*] Johannes A. Russer,[1] Peter Russer,[1] and Christian Jirauschek[1,2]
[1]*TUM School of Computation, Information and Technology, Technical University of Munich, 85748 Garching, Germany*
[2]*TUM Center for Quantum Engineering (ZQE), 85748 Garching, Germany*

(Received 21 October 2022; accepted 25 January 2023; published 15 February 2023)

We present a quantum-mechanical model for a four-wave-mixing Josephson traveling-wave parametric amplifier including substrate losses and associated thermal fluctuations. Under the assumption of a strong undepleted classical pump tone, we derive an analytic solution for the bosonic annihilation operator of the weak signal photon field using temporal equations of motion in a reference timeframe, including chromatic dispersion. From this result, we can predict the asymmetric gain spectrum of a Josephson traveling-wave parametric amplifier due to nonzero substrate losses. We also predict the equivalent added input noise including quantum fluctuations as well as thermal noise contributions. Our results are in excellent agreement with recently published experimental data.

DOI: 10.1103/PhysRevA.107.022612

I. INTRODUCTION

In conventional low-noise microwave amplifiers, amplification is achieved by modulating the channel of a high-electron-mobility transistor. A characteristic measure for the amplifier's performance is the noise temperature, which is defined as the equivalent temperature of a resistor that would produce the same level of Johnson-Nyquist noise [1,2]. The added noise power depends on the channel resistance and easily exceeds the energy of a few tens of microwave photons, even when the circuit is cooled down to cryogenic temperatures [3]. In superconducting quantum computing where the qubit state is probed by ultra-low-power microwave signals, however, quantum-limited [4] noise performance is key for high-fidelity single-shot readouts of quantum information [5]. This and the limited cooling power budget in the lowest-temperature stage of dilution refrigerators render the use of traditional solid-state amplifiers impossible in the context of low-power dispersive qubit readout.

For the detection and amplification of single-photon-level microwave signals, a different type of low-noise amplifier is required where the gain does not originate from modulating a dissipative channel. Parametric amplification is accomplished by nonlinear mixing of the input signal with a strong coherent pump field. The wave-mixing interaction is nondissipative and thus achieves superior noise performance [6]. Superconducting parametric amplifiers based on the nonlinear kinetic inductance of Josephson junctions [7] approach the quantum noise limit [4] with very little power dissipation. Hence, they are used as first-stage amplifiers in the readout of superconducting qubits [8–10]. In recent years, research on parametric amplifiers gained a lot of momentum due to the growing interest in superconducting quantum computing. The first experimental evidence for the feasibility of parametric amplification with Josephson junctions was already obtained in 1967 [11]. The first theoretical study was given in [12]. General energy relations for frequency conversion in nonlinear reactances have been found in [13], which are needed to describe dc-pumped parametric amplification [14]. An exhaustive review of different microwave parametric amplifier designs in the context of quantum information experiments is given in [15]. In a typical architecture, a single Josephson junction is coupled to a resonator in order to increase the gain of the amplifier by increasing the interaction time of the signal and pump modes. The microwave resonator, however, limits the bandwidth of the amplifier to the resonator bandwidth. The amplifier resonator is operated in reflection mode, where a bulky microwave circulator needs to be used to separate the respective input and output waves [16]. Both limitations, the limited bandwidth as well as the need for a circulator, can be overcome by using a traveling-wave type architecture as proposed by [17], where Josephson junctions are periodically embedded in a microwave transmission line. Josephson traveling-wave parametric amplifiers (JTWPAs) achieve large gain by increasing the interaction time of the signal and pump modes through a large propagation distance [18,19]. The interaction along the nonlinear transmission line shows a strong phase sensitivity. Thus, optimum parametric gain can only be achieved if the amplification process is phase matched by careful dispersion engineering [20–22].

In [23], the Josephson-embedded nonlinear transmission line is described by a classical nonlinear wave equation. The operation principle was modeled using coupled-mode equations (CMEs), allowing one to straightforwardly calculate the amplifier's gain spectrum. Single-photon applications at ultralow temperatures, however, necessitate a quantum-mechanical treatment of the device. Quantum-mechanical models for Josephson circuits can be obtained in the framework of quantum circuit theory [24–26], where the term "mesoscopic physics" has been coined for systems which contain a large number of electrons and yet show distinct quantum features [27].

Quantum models for lumped-element Josephson parametric amplifiers (JPAs) have been investigated in [14,28,29].

*michael.haider@tum.de; https://www.ee.cit.tum.de/cph.

Dissipation and thermal noise in the JPA were introduced phenomenologically in [30] by coupling the inner degrees of freedom to a bath. A Hamiltonian description of a JTWPA using continuous-mode operators was derived in [31]. A similar discrete-mode mesoscopic Hamiltonian was presented in [32], which serves as a starting point for the investigations of the present paper. For the derivation of the CMEs in [20,23] and the quantum descriptions in [31,32] nondissipative parametric amplification was assumed, i.e., all losses were neglected.

In this paper, we extend the Hamiltonian framework from [31,32] in order to treat noise and dissipation, mainly arising from substrate losses along the transmission line since the transmission line conductor itself is in a superconducting state. Noise and dissipation are included in the Hamiltonian by phenomenologically coupling the signal and idler modes to a bath, consisting of an infinite number of quantum harmonic oscillators [33]. The coupling constants depend on the substrate material and can be represented by different coupling models [34]. Having a dissipative model for a Josephson traveling-wave parametric amplifier at hand enables studying the frequency-dependent attenuation and noise performance close to the quantum limit. Fluctuations and dissipation in quantum traveling-wave parametric amplifiers were studied in [35] using input-output theory as well as a distributed loss model. In the following, we present an analytic solution for the photon field annihilation operator in a Josephson-embedded transmission line including substrate losses and additional thermal noise. From there we calculate expressions for the amplifier gain and the added input noise which both match experimental results [36]. We predict an added input noise equivalent to approximately 1.3 excess photons, which is in excellent agreement with recent experimental observations [36].

First, we introduce a circuit model of a dissipative-dispersive Josephson junction-embedded transmission line in Sec. II. We then discuss the traveling-wave mode quantization in Sec. III and introduce the JTWPA dispersion relation along with a reference timeframe in Sec. IV. In Sec. V we introduce our four-wave-mixing Hamiltonian. Afterwards, the Heisenberg equations of motion are derived within the moving reference timeframe in Sec. VI. The resulting equations for the photon field are then solved in order to get an analytic expression for the signal mode annihilation operator under a strong classical pump approximation in Sec. VII. Next, we present analytic results for the gain profile and the temporal dynamics of an exemplary JTWPA structure from the literature [20,32] including substrate losses in Sec. VIII. In Sec. IX we derive an analytic expression for the number of added noise photons due to thermal fluctuations. We conclude the section with a discussion on the equivalent added input noise for an experimental structure [36], where our theoretical predictions are found to be in excellent agreement with their observations.

II. QUANTUM-MECHANICAL TREATMENT OF A DISSIPATIVE JTWPA

Consider a superconducting transmission line with periodically embedded identical Josephson-junction loadings. The distance between the Josephson nonlinearities is small compared to the wavelength under consideration, which allows for a continuum treatment of the Josephson-embedded transmission line [23]. A circuit representation of the unit cell of such a structure is given in Fig. 1. As the transmission line itself is in a superconducting state, losses and thermal fluctuations only occur due to substrate imperfections, which are included in terms of the resistor and the associated noise current source in the circuit model in Fig. 1, highlighted in orange (light gray) color. In order to derive a quantum model of the continuous dissipative nonlinear transmission line, the resistor and the associated noise current source are modeled in terms of a distributed Markovian heat bath, consisting of an infinite number of harmonic oscillators with thermal initial occupations. It has been shown in [20] that the gain and bandwidth of Josephson traveling-wave parametric amplifiers can be significantly improved by dispersion engineering using resonant phase matching (RPM). Resonant phase matching can be included using periodically embedded *LC* resonators, which are capacitively coupled to the transmission line. The resonators tailor the dispersion relation such that the total phase mismatch along the transmission line remains small over a large bandwidth. In Fig. 1, and throughout the rest of this paper, C' is the ground capacitance per unit length of the transmission line, $L_{\mathrm{J},0}$ and C_{J} are the linear inductance and intrinsic capacitance of the Josephson junctions, Δz is the length of a single unit cell, C_{c} is the RPM coupling capacitance, and C_{r} and L_{r} are the RPM resonator capacitance and inductance. Note that the transmission line inductance has been neglected, as it can be easily included into the linear Josephson inductance.

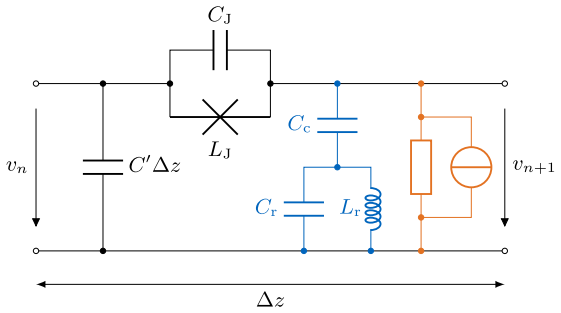

FIG. 1. Unit cell of a JTWPA. Resonant phase matching and a resistive representation of the bath are highlighted in blue (dark gray) and orange (gray) color, respectively.

III. QUANTIZATION OF DISCRETE AND CONTINUOUS MODES

A discrete-mode mesoscopic Hamiltonian for a nondissipative Josephson-embedded transmission line has been derived in [32]. For the quantum-mechanical model in this paper we take a similar approach, where we however consider a continuous mode spectrum in order to derive a consistent noise model in terms of a noise spectral density [37,38]. We use canonical quantization of right-moving traveling-wave modes [27], where the magnetic flux through the Josephson element $\Delta\Phi_{\mathrm{J}}$ and the conjugate charge Q in the ground capacitance per unit length C' are used as canonical pair

of variables, defined over a continuous spatial argument z. Assuming a monochromatic right-traveling wave propagating through a transmission line, we can describe the voltage operator by

$$\hat{V}(z,t) = \hat{c}(z)\, e^{ik(\omega)z - i\omega t} + \text{H.c.}, \tag{1}$$

where $\hat{c}(z)$ is the amplitude operator, ω is the angular frequency of the propagating wave, $k(\omega)$ is the associated wave number, and H.c. denotes the Hermitian conjugate.

A right-traveling wave where the voltage is defined over a continuous frequency spectrum, on the other hand, can be decomposed into monochromatic plane-wave contributions in terms of the inverse Fourier transform,

$$\hat{V}(z,t) = \frac{1}{\sqrt{2\pi}} \int_{-\infty}^{\infty} \hat{c}_{\omega'}\, e^{ik(\omega')z - i\omega' t} d\omega', \tag{2}$$

where the spectral Fourier coefficient operator $\hat{c}_{\omega'}$ can be obtained by means of the Fourier transform of the voltage operator:

$$\hat{c}_{\omega'}(z) = \frac{1}{\sqrt{2\pi}} \int_{-\infty}^{\infty} \hat{V}(z,t)\, e^{-ik(\omega')z + i\omega' t} dt. \tag{3}$$

Hence, monochromatic right-traveling wave amplitude operators can be represented by the spectral coefficient operators:

$$\begin{aligned} \hat{c}_{\omega'} &= \frac{1}{\sqrt{2\pi}} \int_{-\infty}^{\infty} \hat{c}(z)\, e^{i[k(\omega) - k(\omega')]z}\, e^{-i(\omega - \omega')t} dt \\ &= \sqrt{2\pi}\hat{c}(z)\delta(\omega' - \omega). \end{aligned} \tag{4}$$

In the following, relation (4) will be used to translate continuous frequency amplitude operators to their monochromatic limits.

IV. DISPERSION AND REFERENCE TIMEFRAME

Traveling-wave amplitudes inside a dispersionless nonlinear transmission line exhibit space-time translation invariance [39], i.e.,

$$A(z,t) = \hat{A}\left(0, t - \frac{z}{v}\right) = A(z - vt, 0), \tag{5}$$

with the spatial argument z and the frequency-independent propagation velocity v. Thus, the evolution of a corresponding wave amplitude operator $\hat{A}(z,t)$ can be described by either a spatial or a temporal dependence:

$$\hat{A}(z,t) \to \hat{A}(z) \Longleftrightarrow \hat{A}\left(t = \frac{z}{v}\right), \tag{6}$$

where again only right-propagating waves are taken into account. In case of a dispersive transmission line, the phase velocity $v_{\text{ph}}(\omega) = \omega/k(\omega)$ is frequency dependent, where $k(\omega)$ represents the dispersion relation. As each mode now travels at a different velocity, distinct frequency components arrive at a certain location x at different times. In other words, when looking at a certain location x along the transmission line, each mode travels within its own frequency-dependent timeframe. The corresponding timeframes $t(\omega)$ are considered to be frequency-dependent functions which are given by $t(\omega) = z/v_{\text{ph}}(\omega)$. Therefore, the system operators can be described similar to the dispersionless case, by a frequency-dependent time argument:

$$\hat{a}_\omega(z) \to \hat{a}_\omega\left(t(\omega) = \frac{z}{v_{\text{ph}}(\omega)}\right). \tag{7}$$

This way, the spatial dependence of the system annihilation operator $\hat{a}_\omega$ can be expressed by a temporal dependence which permits the use of Heisenberg's equations of motion for calculating the temporal evolution of the system. However, since the Heisenberg equations for different modes are given by means of a frequency-dependent and thus mode-dependent timeframe $t(\omega)$, it is difficult to find analytic solutions. In order to circumvent this problem, we introduce a frequency-independent reference velocity $v_{\text{r}} = \sqrt{\Delta z/L_{\text{J},0}C'}$ with a corresponding reference timeframe $t_{\text{r}} = z/v_{\text{r}}$ which is associated with a wave propagating in a dispersionless ideal transmission line with capacitance C' and inductance $L_{\text{J},0}$ per unit length, respectively. Accordingly, we can define the translation between the reference and phase timeframes by $\partial t(\omega)/\partial t_{\text{r}} = \sqrt{\Lambda(\omega)}$. The dimensionless dispersion factor $\Lambda(\omega)$ is given by

$$\Lambda(\omega) = \frac{1 + \sqrt{1 + \frac{1}{\omega^2 R^2 C'^2 \Delta z^2}}}{2(1 - \omega^2 L_{\text{J},0} C_{\text{J}})} \approx \frac{1}{1 - \omega^2 L_{\text{J},0} C_{\text{J}}}, \tag{8}$$

and may include dispersion due to the intrinsic substrate resistance R, the shunt capacitance C', as well as the Josephson capacitance C_{J}. However, the resistive contributions can usually be neglected because R gets very large for typical substrate materials and signal frequencies, and thus the square-root term in (8) is close to unity. Note that, different from [32], the nonlinearity of the Josephson inductance is not explicitly taken into account for deriving the dispersion factor $\Lambda(\omega)$, where we only use the linear Josephson inductance $L_{\text{J},0}$. Ignoring substrate losses, however, (8) exactly matches the dispersion relation in [20].

V. FOUR-WAVE-MIXING HAMILTONIAN FOR A JTWPA

In order to provide a consistent investigation of thermal noise, we construct the system Hamiltonian in terms of operators with a continuous mode spectrum. Hence, we use [27]

$$\hat{V} = \frac{1}{\sqrt{2\pi}} \int_0^{\infty} \sqrt{\frac{\hbar\omega}{2C' v_{\text{ph}}(\omega)}} [\hat{a}_\omega e^{ik(\omega)z - i\omega t} + \text{H.c.}] d\omega,$$

where C' is the ground capacitance per unit length and $v_{\text{ph}}(\omega)$ represents the frequency-dependent phase velocity. Accordingly, the magnetic flux through the Josephson element can be expressed by the operator

$$\begin{aligned} \Delta\hat{\Phi}_{\text{J}} = \frac{1}{\sqrt{2\pi}} \int_0^{\infty} \frac{k(\omega)\Delta z}{\omega} \sqrt{\frac{\hbar\omega}{2C' v_{\text{ph}}(\omega)}} \\ \times [\hat{a}_\omega\, e^{ik(\omega)z - i\omega t} + \text{H.c.}] d\omega. \end{aligned} \tag{9}$$

The Hamiltonian of a lossless JTWPA can then be obtained by integrating the Hamiltonian density, i.e., the energy stored in the ground capacitors and in the linear and nonlinear inductances of the Josephson junctions per unit length, over the

entire device length x [32]:

$$\hat{H}_{\mathrm{JTWPA}} = \frac{1}{2\Delta z^2}\int_0^x \left\{\left[\frac{\Delta z}{L_{\mathrm{J},0}}\Delta\hat{\Phi}_{\mathrm{J}} - \frac{\Delta z}{12L_{\mathrm{J},0}\varphi_0^2}\Delta\hat{\Phi}_{\mathrm{J}}^3 + C_{\mathrm{J}}\Delta z\frac{\partial^2\Delta\hat{\Phi}_{\mathrm{J}}}{\partial t}\right]\Delta\hat{\Phi}_{\mathrm{J}} + \frac{1}{C'}\hat{Q}^2\right\}dz, \tag{10}$$

where $\varphi_0 = \hbar/(2e)$ is the reduced magnetic flux quantum, $\hbar$ is the reduced Planck's quantum of action, and e is the elementary charge. The quadratic terms in (10) contribute to the linear part of the system Hamiltonian, while the fourth-order term describes the nonlinearity which is responsible for the four-wave-mixing amplification process. The continuous mode Hamiltonian derived in (10) agrees with the Hamiltonian in Eq. (9) of [31].

The input mode spectrum can be decomposed into weak input signal components $\hat{a}_\omega$, together with a strong pump tone $\hat{a}_{\Omega_\mathrm{p}}$ at a pump frequency of Ω_p. Inserting this decomposition into the Josephson flux operator $\Delta\Phi_\mathrm{J}$ (9) and then inserting the result into the Hamiltonian (10), we obtain the lossless system Hamiltonian in terms of the continuous mode operators $\hat{a}_\omega$ and $\hat{a}_{\Omega_\mathrm{p}}$:

$$\begin{aligned}
\hat{H}_{\mathrm{JTWPA}} = {} & \int_0^\infty \hbar\Omega_\mathrm{p}\hat{a}^\dagger_{\Omega_\mathrm{p}}\hat{a}_{\Omega_\mathrm{p}}d\Omega_\mathrm{p} + \int_0^\infty \hbar\omega\hat{a}^\dagger_\omega\hat{a}_\omega d\omega \\
& - \frac{\hbar^2\Delta z^3}{64\pi^2C'^2L_{\mathrm{J},0}^3I_\mathrm{c}^2}\int_0^\infty\int_0^\infty\int_0^\infty\int_0^\infty \frac{k(\tilde{\Omega}_\mathrm{p})k(\tilde{\Omega}'_\mathrm{p})k(\Omega_\mathrm{p})k(\Omega'_\mathrm{p})\,e^{-i(\tilde{\Omega}'_\mathrm{p}-\tilde{\Omega}_\mathrm{p}+\Omega'_\mathrm{p}-\Omega_\mathrm{p})t}}{\sqrt{\tilde{\Omega}_\mathrm{p}\tilde{\Omega}'_\mathrm{p}\Omega_\mathrm{p}\Omega'_\mathrm{p}}v_{\mathrm{ph}}(\tilde{\Omega}_\mathrm{p})v_{\mathrm{ph}}(\tilde{\Omega}'_\mathrm{p})v_{\mathrm{ph}}(\Omega_\mathrm{p})v_{\mathrm{ph}}(\Omega'_\mathrm{p})}\hat{a}^\dagger_{\tilde{\Omega}_\mathrm{p}}\hat{a}_{\tilde{\Omega}'_\mathrm{p}}\hat{a}^\dagger_{\Omega_\mathrm{p}}\hat{a}_{\Omega'_\mathrm{p}} \\
& \times \int_0^x e^{i[k(\tilde{\Omega}'_\mathrm{p})-k(\tilde{\Omega}_\mathrm{p})+k(\Omega'_\mathrm{p})-k(\Omega_\mathrm{p})]z}\,dz d\tilde{\Omega}_\mathrm{p}d\tilde{\Omega}'_\mathrm{p}d\Omega_\mathrm{p}d\Omega'_\mathrm{p} \\
& - \frac{\hbar^2\Delta z^3}{16\pi^2C'^2L_{\mathrm{J},0}^3I_\mathrm{c}^2}\int_0^\infty\int_0^\infty\int_0^\infty\int_0^\infty \frac{k(\omega)k(\omega')k(\Omega_\mathrm{p})k(\Omega'_\mathrm{p})\,e^{-i(\omega'-\omega+\Omega'_\mathrm{p}-\Omega_\mathrm{p})t}}{\sqrt{\omega\omega'\Omega_\mathrm{p}\Omega'_\mathrm{p}}v_{\mathrm{ph}}(\omega)v_{\mathrm{ph}}(\omega')v_{\mathrm{ph}}(\Omega_\mathrm{p})v_{\mathrm{ph}}(\Omega'_\mathrm{p})}\hat{a}^\dagger_\omega\hat{a}_{\omega'}\hat{a}^\dagger_{\Omega_\mathrm{p}}\hat{a}_{\Omega'_\mathrm{p}} \\
& \times \int_0^x e^{i[k(\omega')-k(\omega)+k(\Omega'_\mathrm{p})-k(\Omega_\mathrm{p})]z}\,dz d\omega d\omega' d\Omega_\mathrm{p}d\Omega'_\mathrm{p} \\
& - \frac{\hbar^2\Delta z^3}{32\pi^2C'^2L_{\mathrm{J},0}^3I_\mathrm{c}^2}\int_0^\infty\int_0^\infty\int_0^\infty\int_0^\infty \left[\frac{k(\omega)k(\omega')k(\Omega_\mathrm{p})k(\Omega'_\mathrm{p})\,e^{-i(-\omega-\omega'+\Omega_\mathrm{p}+\Omega'_\mathrm{p})t}}{\sqrt{\omega\omega'\Omega_\mathrm{p}\Omega'_\mathrm{p}}v_{\mathrm{ph}}(\omega)v_{\mathrm{ph}}(\omega')v_{\mathrm{ph}}(\Omega_\mathrm{p})v_{\mathrm{ph}}(\Omega'_\mathrm{p})}\hat{a}^\dagger_\omega\hat{a}^\dagger_{\omega'}\hat{a}_{\Omega_\mathrm{p}}\hat{a}_{\Omega'_\mathrm{p}}\right. \\
& \times \left.\int_0^x e^{i[-k(\omega)-k(\omega')+k(\Omega_\mathrm{p})+k(\Omega'_\mathrm{p})]z} + \mathrm{H.c.}\right]dz d\omega d\omega' d\Omega_\mathrm{p}d\Omega'_\mathrm{p},
\end{aligned} \tag{11}$$

where we have dropped the nonresonant and fast rotating terms. The first line in Eq. (11) describes the propagation of the free photon fields. The second and third lines describe self-phase modulation and the following two lines represent cross-phase modulation of the strong pump tone and the weak signal spectrum. Finally, the last two lines in Eq. (11) describe the actual parametric amplification mechanism due to a nonlinear four-wave-mixing process. The amplification of a signal with frequency ω relies on the annihilation of two pump photons at frequencies Ω_p and Ω'_p, while creating an additional signal photon at frequency ω and an idler photon at ω'.

In order to add losses and noise due to the imperfect substrate isolation to our model, we introduce a phenomenological heat bath, representing an environmental photon field [33]. The heat bath models the dielectric and resistive substrate losses, which are represented by the orange (light gray) resistor in Fig. 1. The bath coupling, however, is bidirectional such that thermally excited photons are introduced within the system in terms of the fluctuation-dissipation theorem [40]. The coupling constants of the heat bath can be related to resistive and dielectric substrate losses by means of expanding the substrate conductivity in a Foster representation [41], i.e., an infinite series of harmonic oscillators [27]. These harmonic oscillators are described by bath creation and annihilation operators $\hat{b}^\dagger_m$ and $\hat{b}_m$ with closely spaced frequencies ω_m. The Hamiltonian describing the bath photon field is given by

$$\hat{H}_{\mathrm{bath}} = \sum_m \hbar\omega_m\int_0^\infty \hat{b}^\dagger_m(\omega)\hat{b}_m(\omega)d\omega, \tag{12}$$

where we performed a Fourier transform of each bath mode and omitted the zero-point energy. The exchange of energy between the heat bath and the system is formulated in terms of a linear coupling Hamiltonian:

$$\hat{H}_{\mathrm{coupling}} = \sum_m \hbar\int_0^\infty [\kappa_m(\omega)\hat{b}^\dagger_m(\omega)\hat{a}_\omega + \mathrm{H.c.}]d\omega \tag{13}$$

with the coupling coefficients $\kappa_m(\omega)$, describing the interaction strength of the mth bath mode and the system, respectively. The total Hamiltonian for a dissipative JTWPA is then given by

$$\hat{H}_{\mathrm{total}} = \hat{H}_{\mathrm{JTWPA}} + \hat{H}_{\mathrm{bath}} + \hat{H}_{\mathrm{coupling}}. \tag{14}$$

Note that within this model, the heat bath is only coupled to the weak signal photon field $\hat{a}_\omega$ and not to the strong pump tone $\hat{a}_{\Omega_\mathrm{p}}$. Hence, losses and noise in the pump tone are being neglected.

The total Hamiltonian $\hat{H}_{\text{total}} = \hat{H}_0 + \hat{H}_1$ is split into an unperturbed part:

$$\hat{H}_0 = \int_0^\infty \hbar\Omega_\text{p}\hat{a}^\dagger_{\Omega_\text{p}}\hat{a}_{\Omega_\text{p}}d\Omega_\text{p} + \int_0^\infty \hbar\omega\hat{a}^\dagger_\omega\hat{a}_\omega d\omega, \tag{15}$$

which represents the free photon field propagation of the pump and weak signal modes, and a perturbative part $\hat{H}_1$ consisting of the remaining terms. The perturbative part hence contains the descriptions for self- and cross-phase-modulation of the strong pump field, the nonlinear four-wave-mixing interaction, as well as losses and noise due to the heat bath. We use the unperturbed Hamiltonian $\hat{H}_0$ to transform the weak photon field operators to a corotating Heisenberg-interaction frame [42], given by

$$\hat{\tilde{a}}_\omega = e^{-i\hat{H}_0 t/\hbar}\hat{a}_\omega e^{i\hat{H}_0 t/\hbar} = \hat{a}_\omega e^{i\omega t}. \tag{16}$$

Within this corotating frame (16), the total Hamiltonian is given in terms of the perturbation Hamiltonian $\hat{H}_1$ according to

$$\hat{\tilde{H}}_1 = e^{i\hat{H}_0 t/\hbar}\hat{H}_1 e^{-i\hat{H}_0 t/\hbar}. \tag{17}$$

Equation (17) describes the dynamics of a JTWPA including environmental coupling in a corotating frame according to the perturbations in $\hat{H}_1$. However, it is difficult to derive the temporal equations of motion of the photon field modes directly from this Hamiltonian, due to the dispersion along the transmission line. Since the amplification mechanism is based on parametric conversion of two pump photons at frequencies Ω_p and Ω'_p into a signal photon at the desired frequency ω and an additional idler photon with frequency ω', such that $\Omega_\text{p} + \Omega'_\text{p} = \omega + \omega'$, we assume a strong discrete degenerate pump mode with a single pump frequency $\Omega_\text{p} = \Omega'_\text{p} = \omega_\text{p}$, similar to [31,32]. Hence, we take the monochromatic limit of the pump mode according to (4), which yields

$$\sqrt{\frac{\hbar\Omega_\text{p}}{2C'v_\text{ph}(\Omega_\text{p})}}\hat{\tilde{a}}_{\Omega_\text{p}} \to \sqrt{2\pi}\sqrt{\frac{\hbar\omega_\text{p}}{2C'l_\text{q}}}\hat{\tilde{a}}_\text{p}\delta(\Omega_\text{p} - \omega_\text{p}), \tag{18}$$

with the quantization length l_q [32]. Furthermore, we adopt the asymptotic scattering limit treatment from [31] and introduce a unitary operator $\hat{U}$ to describe the time evolution of the system dynamics in a first-order perturbation theory neglecting time ordering [43,44]:

$$\hat{U}(t_0, t) = \exp\left[-\frac{i}{\hbar}\int_{t_0}^t \hat{\tilde{H}}_1(\tau)d\tau\right], \tag{19}$$

which is in the scattering limit equal to

$$\hat{U}(t_0, t) \to \hat{U}(-\infty, \infty) = e^{-i\hat{\tilde{K}}_1/\hbar}. \tag{20}$$

The asymptotic scattering limit implies that we are considering a JTWPA section from $z = 0$ to $z = x$ that is embedded within two semi-infinite perfectly matched ideal linear transmission lines from $z = -\infty$ to $z = 0$ and from $z = x$ to $z = \infty$ [31]. The nonlinear interaction as well as dispersion only occur in the "active" region for $z \in [0, x]$. For the substrate loss and noise terms, we set the coupling strength, represented by the coupling coefficients $\kappa(\omega)$, to zero outside the JTWPA section for $z \in [0, x]$ and neglect reflections at the interfaces. A discussion of the scattering limit and more details about the asymptotic approach can be found in [45]. In the asymptotic scattering limit, together with the discrete pump mode (18), the infinite time integral $\hat{\tilde{K}}_1$ of the total Hamiltonian $\hat{\tilde{H}}_1$ (17) can be simplified to

$$\begin{aligned}\hat{\tilde{K}}_1 = &-\frac{\hbar^2\Delta z^3 k_\text{p}^4}{16C'^2L_{\text{J},0}^3I_\text{c}^2\omega_\text{p}^2 l_\text{q}v_\text{ph}(\omega_\text{p})}\hat{\tilde{a}}^\dagger_\text{p}\hat{\tilde{a}}_\text{p}\hat{\tilde{a}}^\dagger_\text{p}\hat{\tilde{a}}_\text{p}\int_0^x e^{i\Delta k_\text{SPM}z}dz - \frac{\hbar^2\Delta z^3 k_\text{p}^2}{4C'^2L_{\text{J},0}^3I_\text{c}^2\omega_\text{p}l_\text{q}}\int_0^\infty\frac{k^2(\omega)}{\omega v_\text{ph}(\omega)}\hat{\tilde{a}}^\dagger_\omega\hat{\tilde{a}}_\omega\hat{\tilde{a}}^\dagger_\text{p}\hat{\tilde{a}}_\text{p}\int_0^x e^{i\Delta k_\text{XPM}z}dzd\omega \\ &-\frac{\hbar^2\Delta z^3 k_\text{p}^2}{8C'^2L_{\text{J},0}^3I_\text{c}^2\omega_\text{p}l_\text{q}}\left[\int_0^\infty\frac{k(\omega)k(2\omega_\text{p}-\omega)}{\sqrt{\omega(2\omega_\text{p}-\omega)v_\text{ph}(\omega)v_\text{ph}(2\omega_\text{p}-\omega)}}\hat{\tilde{a}}^\dagger_\omega\hat{\tilde{a}}^\dagger_{2\omega_\text{p}-\omega}\hat{\tilde{a}}_\text{p}\hat{\tilde{a}}_\text{p}\int_0^x e^{i\Delta k_\text{4WM}z}dzd\omega + \text{H.c.}\right] \\ &+\int_{-\infty}^\infty\int_0^\infty\sum_m\hbar\omega_m\hat{b}^\dagger_m(\omega)\hat{b}_m(\omega)d\omega dt + \int_{-\infty}^\infty\int_0^\infty\sum_m\hbar[\kappa_m(\omega)\hat{b}^\dagger_m(\omega)\hat{\tilde{a}}_\omega e^{-i\omega t} + \text{H.c.}]d\omega dt.\end{aligned} \tag{21}$$

The spatial phase differences Δk_SPM, Δk_XPM, and Δk_4WM in (21) are given by

$$\begin{aligned}\Delta k_\text{SPM} &= k_\text{p} - k_\text{p} + k_\text{p} - k_\text{p} = 0, \\ \Delta k_\text{XPM} &= k(\omega) - k(\omega) + k_\text{p} - k_\text{p} = 0, \\ \Delta k_\text{4WM} &= 2k_\text{p} - k(\omega) - k(2\omega_\text{p} - \omega).\end{aligned}$$

Note that $k_\text{p} = k(\omega_\text{p})$ is the wave vector at the degenerate pump frequency ω_p. We now exploit the space-time symmetry of the traveling-wave amplitudes as discussed in Sec. IV. Hence, we introduce a reference timeframe t_r, which is related to the total JTWPA length x by $x = v_\text{r}t_\text{r}$, with a reference velocity v_r, chosen as $v_\text{r} = \sqrt{\Delta z/L_{\text{J},0}C'}$. The reference time t_r corresponds to the propagation time of the photon field along a transmission line of length x in the dispersionless case. The dispersion factor $\sqrt{\Lambda(\omega)}$, according to (8), translates this reference propagation time t_r to the frequency-dependent total interaction time $t(\omega)$ for each individual mode. Using the dispersion relation

$$k(\omega) = \frac{\omega}{v_\text{r}}\sqrt{\Lambda(\omega)}, \tag{22}$$

together with $x = v_\text{r}t_\text{r}$, we can also translate between the linear spatial phase mismatch Δk_4WM and the linear temporal phase mismatch $\Delta\Omega_\text{L}$ by

$$\begin{aligned}\Delta k_\text{4WM}x &= [2k_\text{p} - k(\omega) - k(2\omega_\text{p} - \omega)]x \\ &= [2\omega_\text{p}\sqrt{\Lambda(\omega_\text{p})} - \omega\sqrt{\Lambda(\omega)} \\ &\quad - (2\omega_\text{p} - \omega)\sqrt{\Lambda(2\omega_\text{p} - \omega)}]t_\text{r} = \Delta\Omega_\text{L}t_\text{r},\end{aligned} \tag{23}$$

where we define the frequency-dependent linear phase mismatch $\Delta\Omega_{\mathrm{L}}$ in (23) by

$$\Delta\Omega_{\mathrm{L}} = 2\omega_{\mathrm{p}}\sqrt{\Lambda(\omega_{\mathrm{p}})} - \omega\sqrt{\Lambda(\omega)} - (2\omega_{\mathrm{p}} - \omega)\sqrt{\Lambda(2\omega_{\mathrm{p}} - \omega)},$$

accordingly.

VI. TEMPORAL EQUATIONS OF MOTION

With the unitary time-evolution operator from (20), it holds that $\hat{\tilde{a}}_\omega = \hat{U}^\dagger \hat{\tilde{a}}_{\omega,0} \hat{U}$, where $\hat{\tilde{a}}_{\omega,0}$ is the weak photon field annihilation operator at some initial time t_0. Hence, the time evolution of the photon field annihilation operator $\hat{\tilde{a}}_\omega$ in the corotating frame is given by

$$\begin{aligned}\frac{\partial \hat{\tilde{a}}_\omega}{\partial t_{\mathrm{r}}} &= \frac{d\hat{U}^\dagger}{dt_{\mathrm{r}}}\hat{\tilde{a}}_{\omega,0}\hat{U} + \hat{U}^\dagger\hat{\tilde{a}}_{\omega,0}\frac{d\hat{U}}{dt_{\mathrm{r}}} \\ &= \frac{i}{\hbar}\frac{d\hat{\tilde{K}}_1}{dt_{\mathrm{r}}}\hat{U}^\dagger\hat{\tilde{a}}_{\omega,0}\hat{U} - \frac{i}{\hbar}\hat{U}^\dagger\hat{\tilde{a}}_{\omega,0}\hat{U}\frac{d\hat{\tilde{K}}_1}{dt_{\mathrm{r}}} \\ &= \frac{i}{\hbar}\frac{d\hat{\tilde{K}}_1}{dt_{\mathrm{r}}}\hat{\tilde{a}}_\omega - \frac{i}{\hbar}\hat{\tilde{a}}_\omega\frac{d\hat{\tilde{K}}_1}{dt_{\mathrm{r}}} \\ &= \frac{i}{\hbar}\left[\frac{d\hat{\tilde{K}}_1}{dt_{\mathrm{r}}}, \hat{\tilde{a}}_\omega\right], \end{aligned} \tag{24}$$

where t_{r} highlights that the time evolution is calculated within the reference timeframe. Thus, within the reference timeframe t_{r}, the system Hamiltonian in the Heisenberg picture is given in terms of the derivative of $\hat{\tilde{K}}_1$ with respect to t_{r}, where the length x of the JTWPA has been replaced by $x = v_{\mathrm{r}}\, t_{\mathrm{r}}$, i.e.,

$$\begin{aligned}\frac{d\hat{\tilde{K}}_1}{dt_{\mathrm{r}}} =& -\frac{\hbar^2\Delta z^3 k_{\mathrm{p}}^4\sqrt{\Lambda(\omega_{\mathrm{p}})}}{16C'^2L_{\mathrm{J},0}^3 I_{\mathrm{c}}^2\omega_{\mathrm{p}}^2 l_{\mathrm{q}}}\hat{\tilde{a}}_{\mathrm{p}}^\dagger\hat{\tilde{a}}_{\mathrm{p}}\hat{\tilde{a}}_{\mathrm{p}}^\dagger\hat{\tilde{a}}_{\mathrm{p}} - \frac{\hbar^2\Delta z^3 k_{\mathrm{p}}^2}{4C'^2L_{\mathrm{J},0}^3 I_{\mathrm{c}}^2\omega_{\mathrm{p}} l_{\mathrm{q}}}\int_0^\infty \frac{k^2(\omega)\sqrt{\Lambda(\omega)}}{\omega}\hat{\tilde{a}}_\omega^\dagger\hat{\tilde{a}}_\omega\hat{\tilde{a}}_{\mathrm{p}}^\dagger\hat{\tilde{a}}_{\mathrm{p}}d\omega \\ &- \frac{\hbar^2\Delta z^3 k_{\mathrm{p}}^2}{8C'^2L_{\mathrm{J},0}^3 I_{\mathrm{c}}^2\omega_{\mathrm{p}} l_{\mathrm{q}}}\left[\int_0^\infty \frac{k(\omega)k(2\omega_{\mathrm{p}}-\omega)[\Lambda(\omega)\Lambda(2\omega_{\mathrm{p}}-\omega)]^{\frac{1}{4}}}{\sqrt{\omega(2\omega_{\mathrm{p}}-\omega)}}\hat{\tilde{a}}_\omega^\dagger\hat{\tilde{a}}_{2\omega_{\mathrm{p}}-\omega}^\dagger\hat{\tilde{a}}_{\mathrm{p}}\hat{\tilde{a}}_{\mathrm{p}}\, e^{i\Delta\Omega_{\mathrm{L}}t_{\mathrm{r}}}d\omega + \mathrm{H.c.}\right] \\ &+ \sum_m \hbar\omega_m\sqrt{\Lambda(\omega_m)}\int_0^\infty \hat{b}_m^\dagger(\omega)\hat{b}_m(\omega)d\omega + \sum_m \hbar\sqrt{\Lambda(\omega_m)}\int_0^\infty [\kappa_m(\omega)\hat{b}_m^\dagger(\omega)\hat{\tilde{a}}_\omega e^{-i\omega\sqrt{\Lambda(\omega_m)}t_{\mathrm{r}}} + \mathrm{H.c.}]d\omega. \end{aligned} \tag{25}$$

Within the reference timeframe t_{r}, equations of motion for the system and bath operators can be obtained from (24) and (25), according to

$$\frac{\partial\hat{\tilde{a}}_{\mathrm{p}}}{\partial t_{\mathrm{r}}} = \frac{i\hbar\Delta z^3 k_{\mathrm{p}}^4\sqrt{\Lambda(\omega_{\mathrm{p}})}}{8C'^2L_{\mathrm{J},0}^3 I_{\mathrm{c}}^2\omega_{\mathrm{p}}^2 l_{\mathrm{q}}}\hat{\tilde{a}}_{\mathrm{p}}^\dagger\hat{\tilde{a}}_{\mathrm{p}}\hat{\tilde{a}}_{\mathrm{p}}, \tag{26}$$

$$\begin{aligned}\frac{\partial\hat{\tilde{a}}_\omega}{\partial t_{\mathrm{r}}} =& \frac{i\hbar\Delta z^3 k_{\mathrm{p}}^2 k^2(\omega)\sqrt{\Lambda(\omega)}}{4C'^2L_{\mathrm{J},0}^3 I_{\mathrm{c}}^2\omega_{\mathrm{p}}\omega l_{\mathrm{q}}}\hat{\tilde{a}}_{\mathrm{p}}^\dagger\hat{\tilde{a}}_{\mathrm{p}}\hat{\tilde{a}}_\omega + \frac{i\hbar\Delta z^3 k_{\mathrm{p}}^2 k(\omega)k(2\omega_{\mathrm{p}}-\omega)[\Lambda(\omega)\Lambda(2\omega_{\mathrm{p}}-\omega)]^{\frac{1}{4}}}{8C'^2L_{\mathrm{J},0}^3 I_{\mathrm{c}}^2\omega_{\mathrm{p}}\sqrt{\omega(2\omega_{\mathrm{p}}-\omega)}l_{\mathrm{q}}}\hat{\tilde{a}}_{\mathrm{p}}\hat{\tilde{a}}_{\mathrm{p}}\hat{\tilde{a}}_{2\omega_{\mathrm{p}}-\omega}^\dagger\, e^{i\Delta\Omega_{\mathrm{L}}t_{\mathrm{r}}} \\ &- i\sum_m \kappa_m(\omega)\sqrt{\Lambda(\omega_m)}\,\hat{b}_m e^{i\omega\sqrt{\Lambda(\omega_m)}t_{\mathrm{r}}}, \end{aligned} \tag{27}$$

$$\frac{\partial\hat{b}_m}{\partial t_{\mathrm{r}}} = -i\omega_m\sqrt{\Lambda(\omega_m)}\,\hat{b}_m - i\kappa_m(\omega)\sqrt{\Lambda(\omega_m)}\,\hat{\tilde{a}}_\omega e^{-i\omega\sqrt{\Lambda(\omega_m)}t_{\mathrm{r}}}. \tag{28}$$

As the pump mode is by orders of magnitude stronger than the weak signal photon field, we furthermore assume that the pump tone can be approximated by a classical mode amplitude, i.e.,

$$\sqrt{\frac{\hbar}{2C'\omega_{\mathrm{p}}l_{\mathrm{q}}}}\hat{\tilde{a}}_{\mathrm{p}} \to -\frac{i}{2}A_{\mathrm{p}}. \tag{29}$$

Consequently, we also neglect pump depletion, i.e., photons that are being annihilated in the pump mode to create a signal and an idler photon by four-wave mixing will not deplete the pump mode [32]. This is a bold assumption, as it violates energy conservation, but it can be justified by the huge difference in the number of photons in the weak signal field compared to the strong classical pump tone. However, it allows us to construct analytic solutions for the temporal evolution of the photon field, as we will see in the following. We also neglect leakage of pump power to higher harmonics [46]. Within our model, terms of smaller than second order in the pump amplitude are neglected.

The classical pump approximation (29), while neglecting pump depletion [32], drastically simplifies the resulting equation of motion. Equations (26) to (28) together with (29) result in a set of approximated first-order temporal Heisenberg equations, given by

$$\frac{\partial A_{\mathrm{p}}}{\partial t_{\mathrm{r}}} = i\theta_{\mathrm{p}}\sqrt{\Lambda(\omega_{\mathrm{p}})}A_{\mathrm{p}}, \tag{30}$$

$$\begin{aligned}\frac{\partial\hat{\tilde{a}}_\omega}{\partial t_{\mathrm{r}}} =& \, i\theta(\omega)\sqrt{\Lambda(\omega)}\,\hat{\tilde{a}}_\omega - i\chi' A_{\mathrm{p}}^2[\Lambda(\omega)\Lambda(2\omega_{\mathrm{p}}-\omega)]^{\frac{1}{4}} \\ &\times\hat{\tilde{a}}_{2\omega_{\mathrm{p}}-\omega}^\dagger e^{i\Delta\Omega_{\mathrm{L}}t_{\mathrm{r}}} - i\sum_m \kappa_m(\omega)\sqrt{\Lambda(\omega_m)}\,\hat{b}_m e^{i\omega\sqrt{\Lambda(\omega_m)}t_{\mathrm{r}}}, \end{aligned} \tag{31}$$

$$\frac{\partial \hat{b}_m}{\partial t_\mathrm{r}} = -i\omega_m\sqrt{\Lambda(\omega_m)}\,\hat{b}_m - i\kappa_m(\omega)\sqrt{\Lambda(\omega_m)}\hat{\tilde{a}}_\omega e^{-i\omega\sqrt{\Lambda(\omega_m)}t_\mathrm{r}}. \tag{32}$$

Self-phase modulation of the strong monochromatic classical pump amplitude is described by means of θ_p and cross-phase modulation is included in the weak signal modes through $\theta(\omega)$. The coefficient for cross-phase modulation $\theta(\omega)$ is given by

$$\theta(\omega) = \frac{k_\mathrm{p}^2\Delta z^2\Lambda(\omega)\omega}{8L_{\mathrm{J},0}^2 I_\mathrm{c}^2}|A_{\mathrm{p},0}|^2, \tag{33}$$

while the one for self-phase modulation $\theta_\mathrm{p} = \theta(\omega_\mathrm{p})/2$. Here, $|A_{\mathrm{p},0}|$ is the initial magnitude of the monochromatic pump tone at the amplifier input. The four-wave-mixing interaction strength χ' in (31) was summarized as

$$\chi' = \frac{k_\mathrm{p}^2\Delta z^2\sqrt{\Lambda(\omega)\Lambda(2\omega_\mathrm{p}-\omega)}\sqrt{\omega(2\omega_\mathrm{p}-\omega)}}{16L_{\mathrm{J},0}^2 I_\mathrm{c}^2}. \tag{34}$$

The wave number k_p can be obtained from the reference velocity v_r, considering the dispersion factor given in (8):

$$k(\omega) = \omega\sqrt{\frac{L_{\mathrm{J},0}C'}{\Delta z}\Lambda(\omega)}, \tag{35}$$

where $k_\mathrm{p} = k(\omega_\mathrm{p})$. A detailed derivation of the dispersion relation and the wave number of a dissipative transmission line is given in [47].

As we neglect pump depletion and losses, (30) is decoupled from the rest of the system and can be solved independently. Hence, by formally integrating (30), the temporal evolution of the classical pump amplitude is given by

$$A_\mathrm{p} = A_{\mathrm{p},0}\, e^{i\theta_\mathrm{p}\sqrt{\Lambda(\omega_\mathrm{p})}t_\mathrm{r}}. \tag{36}$$

Therefore, the amplitude of the monochromatic strong undepleted classical pump mode in (36) can be considered constant over space and time, $|A_\mathrm{p}| = |A_{\mathrm{p},0}|$.

The bath mode operators $\hat{b}_m$ can be expressed in terms of the initial bath amplitudes $\hat{b}_{m,0}$ and the mode operators $\hat{\tilde{a}}_\omega$ by formally integrating (32) [48]:

$$\hat{b}_m = \hat{b}_{m,0}e^{-i\omega_m\sqrt{\Lambda(\omega_m)}t_\mathrm{r}} - i\kappa_m(\omega)\sqrt{\Lambda(\omega_m)} \times \int_0^{t_\mathrm{r}} \hat{\tilde{a}}_\omega(t_\mathrm{r}-\tau)e^{-i\omega\sqrt{\Lambda(\omega_m)}(t_\mathrm{r}-\tau)}e^{-i\omega_m\sqrt{\Lambda(\omega_m)}\tau}d\tau. \tag{37}$$

Inserting (37) and the solution for the classical pump amplitude (36) into the equation of motion for the weak photon field operators $\hat{\tilde{a}}_\omega$, we obtain

$$\frac{\partial \hat{\tilde{a}}_\omega}{\partial t_\mathrm{r}} = i\theta(\omega)\sqrt{\Lambda(\omega)}\,\hat{\tilde{a}}_\omega - i\chi' A_{\mathrm{p},0}^2[\Lambda(\omega)\Lambda(2\omega_\mathrm{p}-\omega)]^{\frac{1}{4}}\hat{\tilde{a}}_{2\omega_\mathrm{p}-\omega}^\dagger e^{i[2\theta_\mathrm{p}\sqrt{\Lambda(\omega_\mathrm{p})}+\Delta\Omega_\mathrm{L}]t_\mathrm{r}} - i\sum_m \kappa_m(\omega)\sqrt{\Lambda(\omega_m)}\,\hat{b}_{m,0} \times e^{-i[\omega_m\sqrt{\Lambda(\omega_m)}-\omega\sqrt{\Lambda(\omega_m)}]t_\mathrm{r}} - \sum_m \kappa_m^2(\omega)\Lambda(\omega_m)\int_0^{t_\mathrm{r}}\hat{\tilde{a}}_\omega(t_\mathrm{r}-\tau)e^{-i[\omega_m\sqrt{\Lambda(\omega_m)}-\omega\sqrt{\Lambda(\omega_m)}]\tau}d\tau. \tag{38}$$

Here, the first line in (38) expresses the evolution of the unperturbed system, together with the four-wave-mixing interaction due to the Josephson nonlinearity. The second and the third line represent fluctuation and dissipation, respectively.

In a next step, we assume a memoryless Markovian system, i.e., the interference time is much smaller than the time over which significant changes in phase and amplitude of $\hat{a}_\omega$ occur [33,49]. In the context of Josephson parametric amplifiers, a similar derivation has already been given in [30]; however, there it was done for discrete mode operators in a lumped-element JPA resonator. Distributed losses in quantum traveling-wave parametric amplifiers have been studied in [35,50], using a continuous input-output theory. As the bath mode frequencies ω_m are closely spaced, we replace the sum over m bath modes by an integral over a continuous frequency argument Ω_b:

$$\sum_m \to \int_{-\infty}^{\infty} d\Omega_\mathrm{b}\mathcal{D}(\Omega_\mathrm{b}), \tag{39}$$

where $\mathcal{D}(\Omega_\mathrm{b})$ is the one-dimensional density of states. Here, the heat bath is modeled as a distributed resistance in terms of a closely spaced ensemble of harmonic oscillators, that is coupled to the system in each unit cell. We define frequency-dependent damping factors by

$$\gamma(\omega) = 2\pi\mathcal{D}(\omega)\kappa^2(\omega)\sqrt{\Lambda(\omega)}, \tag{40}$$

where the translation factor $\sqrt{\Lambda(\omega)}$ ensures that the correct propagation time or length is taken into account for each mode when calculating the losses. In order to further simplify the equation of motion of the weak photon field operators, we again switch to a corotating frame $\hat{A}_\omega = \hat{\tilde{a}}_\omega \exp\{-i[\theta(\omega)\sqrt{\Lambda(\omega)} + \Delta\Omega/2]t_\mathrm{r}\}$, with the frequency-dependent total phase mismatch:

$$\Delta\Omega = 2[\omega_\mathrm{p}+\theta_\mathrm{p}]\sqrt{\Lambda(\omega_\mathrm{p})} - [\omega+\theta(\omega)]\sqrt{\Lambda(\omega)} - [2\omega_\mathrm{p}-\omega+\theta(2\omega_\mathrm{p}-\omega)]\sqrt{\Lambda(2\omega_\mathrm{p}-\omega)}. \tag{41}$$

Within this corotating frame, we obtain a system of two coupled first-order inhomogeneous differential equations for the weak photon field operators $\hat{A}_\omega$, one centered at the signal frequency ω, and one at the idler frequency $2\omega_\mathrm{p}-\omega$. The resulting system of equations can be written in matrix

form as

$$\begin{bmatrix} \frac{\partial \hat{A}_\omega}{\partial t_r} \\ \frac{\partial \hat{A}^\dagger_{2\omega_p-\omega}}{\partial t_r} \end{bmatrix} = \begin{bmatrix} -\frac{\gamma(\omega)}{2} - \frac{i\Delta\Omega}{2} & -i\chi' A_{p,0}^2[\Lambda(\omega)\Lambda(2\omega_p-\omega)]^{\frac{1}{4}} \\ i\chi'^* A_{p,0}^{*\,2}[\Lambda(\omega)\Lambda(2\omega_p-\omega)]^{\frac{1}{4}} & -\frac{\gamma(2\omega_p-\omega)}{2} + \frac{i\Delta\Omega}{2} \end{bmatrix} \begin{bmatrix} \hat{A}_\omega \\ \hat{A}^\dagger_{2\omega_p-\omega} \end{bmatrix} + \begin{bmatrix} \hat{f}(\omega) \\ \hat{f}^\dagger(2\omega_p-\omega) \end{bmatrix}. \tag{42}$$

While losses are directly incorporated in the system matrix in (42) through the damping factors $\gamma(\omega)$, noise is included by the inhomogeneous fluctuation operators $\hat{f}(\omega)$ and $\hat{f}(2\omega_p-\omega)$. These fluctuation operators are given by

$$\hat{f}(\omega) = -i\sum_m \kappa_m(\omega)\sqrt{\Lambda(\omega)}\hat{b}_{m,0}(\omega)e^{-i[(\omega_m-\omega)\sqrt{\Lambda(\omega_m)}+\theta(\omega)\sqrt{\Lambda(\omega)}+\frac{\Delta\Omega}{2}]t_r}. \tag{43}$$

VII. ANALYTIC SOLUTION FOR THE PHOTON FIELD OPERATOR

The inhomogeneous system of differential equations (42) can be solved analytically by standard methods. By evaluating an eigenvector basis of the system matrix in (42), the time evolution of the weak signal photon field annihilation operator $\hat{A}_\omega$ is found as

$$\begin{aligned}
\hat{A}_\omega &= \left[\cosh(gt_r) - \frac{\gamma(\omega)-\gamma(2\omega_p-\omega)+2i\Delta\Omega}{4g}\sinh(gt_r)\right]\hat{A}_{\omega,0}e^{-\frac{\gamma(\omega)+\gamma(2\omega_p-\omega)}{4}t_r} - \frac{i\chi' A_{p,0}^2[\Lambda(\omega)\Lambda(2\omega_p-\omega)]^{\frac{1}{4}}}{g}\sinh(gt_r)\hat{A}^\dagger_{2\omega_p-\omega,0} \\
&\quad\times e^{-\frac{\gamma(\omega)+\gamma(2\omega_p-\omega)}{4}t_r} + \int_0^{t_r}\left\{\cosh[g(t_r-\tau)] - \frac{\gamma(\omega)-\gamma(2\omega_p-\omega)+2i\Delta\Omega}{4g}\sinh[g(t_r-\tau)]\right\}\hat{f}(\omega)\,e^{-\frac{\gamma(\omega)+\gamma(2\omega_p-\omega)}{4}(t_r-\tau)}d\tau \\
&\quad - \int_0^{t_r}\frac{i\chi' A_{p,0}^2[\Lambda(\omega)\Lambda(2\omega_p-\omega)]^{\frac{1}{4}}}{g}\sinh[g(t_r-\tau)]\hat{f}^\dagger(2\omega_p-\omega)\,e^{-\frac{\gamma(\omega)+\gamma(2\omega_p-\omega)}{4}(t_r-\tau)}d\tau \\
&= \zeta_1(\omega,t_r)\hat{A}_{\omega,0}e^{-\frac{\gamma(\omega)+\gamma(2\omega_p-\omega)}{4}t_r} + \zeta_2(\omega,t_r)\hat{A}^\dagger_{2\omega_p-\omega,0}e^{-\frac{\gamma(\omega)+\gamma(2\omega_p-\omega)}{4}t_r} \\
&\quad + \int_0^{t_r}\zeta_1(\omega,t_r-\tau)\hat{f}(\omega)\,e^{-\frac{\gamma(\omega)+\gamma(2\omega_p-\omega)}{4}(t_r-\tau)}d\tau + \int_0^{t_r}\zeta_2(\omega,t_r-\tau)\hat{f}^\dagger(2\omega_p-\omega)\,e^{-\frac{\gamma(\omega)+\gamma(2\omega_p-\omega)}{4}(t_r-\tau)}d\tau,
\end{aligned} \tag{44}$$

with the gain rate

$$g = \sqrt{\left[\frac{\gamma(\omega)-\gamma(2\omega_p-\omega)+2i\Delta\Omega}{4}\right]^2 + |\chi'|^2\left|A_{p,0}^2\right|^2\sqrt{\Lambda(\omega)\Lambda(2\omega_p-\omega)}}. \tag{45}$$

The signal and idler evolution functions $\zeta_1(\omega,t_r)$ and $\zeta_2(\omega,t_r)$ are given by

$$\zeta_1(\omega,t_r) = \cosh(gt_r) - \eta(\omega)\sinh(gt_r), \tag{46}$$

$$\zeta_2(\omega,t_r) = \rho(\omega)\sinh(gt_r), \tag{47}$$

with

$$\eta(\omega) = \frac{\gamma(\omega)-\gamma(2\omega_p-\omega)+2i\Delta\Omega}{4g}, \tag{48}$$

$$\rho(\omega) = -\frac{i\chi' A_{p,0}^2[\Lambda(\omega)\Lambda(2\omega_p-\omega)]^{\frac{1}{4}}}{g}. \tag{49}$$

The first line in (44) represents the amplification of the weak photon field at frequencies around ω due to four-wave mixing. The contribution of the added noise due to the down-conversion of energy from the idler field at $2\omega_p-\omega$ is shown in the second line. Both contributions experience exponential damping by the damping factors $\gamma(\omega)$ and $\gamma(2\omega_p-\omega)$, which are due to losses within the dielectric substrate. The next two lines describe the evolution of thermal fluctuations within the quantum system due to the lossy environment. While the integrals in the last two lines of (44) could be easily evaluated, we refrain from doing so here for the sake of a more streamlined derivation of the second-order moments later on. It can be seen that photons originating from thermal fluctuations experience similar amplification and damping compared to the weak signal photon field.

The gain factor g from (45) describes the amplification of the system per unit time within the reference timeframe $t = t_r$. According to (45), high gain can be achieved by increasing the four-wave-mixing interaction strength χ' as well as the pump amplitude $A_{p,0}$. Thus, JTWPAs are typically operated with pump powers just below the limits set by the critical current of the Josephson junctions [51].

Let us note here that the analytic result must represent a bosonic mode annihilation operator. Thus, one can verify whether the analytic solution $\hat{A}_\omega$ satisfies the bosonic commutation relation. A straightforward calculation shows that the commutation relation is indeed satisfied for the given result, i.e.,

$$[\hat{A}_\omega, \hat{A}^\dagger_{\omega'}] = \hat{A}_\omega\hat{A}^\dagger_{\omega'} - \hat{A}^\dagger_{\omega'}\hat{A}_\omega = \delta(\omega-\omega'). \tag{50}$$

In the dissipationless limit, we recover the well-known condition $|\zeta_1(\omega,t_r)|^2 - |\zeta_2(\omega,t_r)|^2 = 1$ from [31,52], which gives us further confirmation.

VIII. GAIN SPECTRUM AND TEMPORAL EVOLUTION

For both cases with and without RPM, the expected photon number, and hence the gain of the JTWPA, can be obtained by integrating the spectral density, given by the auto- and cross-correlation functions of the photon field operators:

$$\begin{aligned}\langle \hat{A}^{\dagger}_{\omega}\hat{A}_{\omega'}\rangle = &\big[\zeta_1^*(\omega,t_r)\zeta_1(\omega',t_r)\langle \hat{A}^{\dagger}_{\omega,0}\hat{A}_{\omega',0}\rangle + \zeta_2^*(\omega,t_r)\zeta_2(\omega',t_r)\big\langle \hat{A}_{2\omega_p-\omega,0}\hat{A}^{\dagger}_{2\omega_p-\omega',0}\big\rangle \\ &+ \zeta_1^*(\omega,t_r)\zeta_2(\omega',t_r)\big\langle \hat{A}^{\dagger}_{\omega,0}\hat{A}^{\dagger}_{2\omega_p-\omega',0}\big\rangle + \zeta_2^*(\omega,t_r)\zeta_1(\omega',t_r)\big\langle \hat{A}_{2\omega_p-\omega,0}\hat{A}_{\omega',0}\big\rangle\big] e^{-\frac{\gamma(\omega)+\gamma(2\omega_p-\omega)+\gamma(\omega')+\gamma(2\omega_p-\omega')}{4}t_r} \\ &+ \int_0^{t_r}\int_0^{t_r}[\zeta_1^*(\omega,t_r-\tau)\zeta_1(\omega',t_r-\tau')\langle \hat{f}^{\dagger}(\omega)\hat{f}(\omega')\rangle + \zeta_2^*(\omega,t_r-\tau)\zeta_2(\omega',t_r-\tau')\langle \hat{f}(2\omega_p-\omega)\hat{f}^{\dagger}(2\omega_p-\omega')\rangle \\ &+ \zeta_1^*(\omega,t_r-\tau)\zeta_2(\omega',t_r-\tau')\langle \hat{f}^{\dagger}(\omega)\hat{f}^{\dagger}(2\omega_p-\omega')\rangle + \zeta_2^*(\omega,t_r-\tau)\zeta_1(\omega',t_r-\tau')\langle \hat{f}(2\omega_p-\omega)\hat{f}(\omega')\rangle] \\ &\times e^{-\frac{\gamma(\omega)+\gamma(2\omega_p-\omega)}{4}(t_r-\tau)}e^{-\frac{\gamma(\omega')+\gamma(2\omega_p-\omega')}{4}(t_r-\tau')}d\tau d\tau'. \end{aligned} \tag{51}$$

The correlation functions of the noise operators $\hat{f}(\omega)$ in (51) are given by

$$\langle \hat{b}^{\dagger}_{m,0}(\omega)\hat{b}_{n,0}(\omega')\rangle = \bar{n}(\omega_m)\delta_{mn}\delta(\omega-\omega'), \tag{52}$$

where $\bar{n}(\omega_m)$ is the expected occupation of the mth bath mode. Assuming that the heat bath is a photon reservoir in thermal equilibrium at temperature T, the expected photon number in the mth bath mode is given by Bose-Einstein statistics:

$$\bar{n}(\omega_m) = \frac{1}{e^{\hbar\omega_m/(k_B T)}-1}, \tag{53}$$

where k_B is Boltzmann's constant.

We assume that the input photon field has discrete mode spectral densities, given by

$$\langle \hat{A}^{\dagger}_{\omega,0}\hat{A}_{\omega',0}\rangle = N_{s,0}\,\delta(\omega-\omega'), \tag{54}$$

$$\big\langle \hat{A}_{2\omega_p-\omega,0}\hat{A}^{\dagger}_{2\omega_p-\omega',0}\big\rangle = (N_{i,0}+1)\,\delta(\omega-\omega'), \tag{55}$$

with initial correlations

$$\big\langle \hat{A}_{2\omega_p-\omega,0}\hat{A}_{\omega',0}\big\rangle = \big\langle \hat{A}^{\dagger}_{\omega,0}\hat{A}^{\dagger}_{2\omega_p-\omega',0}\big\rangle^* = C_{si,0}\,\delta(\omega-\omega'), \tag{56}$$

where $N_{s,0}$ is the initial photon number of the weak photon field at the discrete signal frequency ω, $N_{i,0}$ is the initial idler photon number at a frequency of $2\omega_p-\omega$, and $C_{si,0}$ is the initial signal-idler mode correlation. Now and in the following, it is important to distinguish between the input and the output modes, as well as the inner degrees of freedom of the amplifier. The input and output of the amplifier are given by a weak signal photon field at a frequency ω with a narrow bandwidth $B_s \ll \omega$. The total photon number at the output of the amplifier within the narrow signal bandwidth B_s, after a reference-mode travel time of t_r, can be evaluated by integrating (51) over frequency:

$$N_{s,t_r} = \int_{\omega-\frac{B_s}{2}}^{\omega+\frac{B_s}{2}} \langle \hat{A}^{\dagger}_{\omega}\hat{A}_{\omega'}\rangle d\omega'. \tag{57}$$

Performing an integration by parts of (57), considering the delta functions in the spectral densities, yields the total photon number N_{s,t_r} at the output, given by

$$\begin{aligned} N_{s,t_r} = &\bar{n}(\omega) + [N_{s,0}-\bar{n}(\omega)]\zeta_1(\omega,t_r)\zeta_1^*(\omega,t_r)e^{-\frac{\gamma(\omega)+\gamma(2\omega_p-\omega)}{2}t_r} + C_{si,0}\zeta_1(\omega,t_r)\zeta_2^*(\omega,t_r)e^{-\frac{\gamma(\omega)+\gamma(2\omega_p-\omega)}{2}t_r} \\ &+ [N_{i,0}+\bar{n}(\omega)+1]\zeta_2(\omega,t_r)\zeta_2^*(\omega,t_r)e^{-\frac{\gamma(\omega)+\gamma(2\omega_p-\omega)}{2}t_r} + C_{si,0}^*\zeta_2(\omega,t_r)\zeta_1^*(\omega,t_r)e^{-\frac{\gamma(\omega)+\gamma(2\omega_p-\omega)}{2}t_r} \\ &+ [\bar{n}(\omega)+\bar{n}(2\omega_p-\omega)+1]\bar{F}(\omega,t_r)e^{-\frac{\gamma(\omega)+\gamma(2\omega_p-\omega)}{2}t_r}, \end{aligned} \tag{58}$$

where the evolution of the independent part $\bar{F}(\omega)$ in the third line of (58) is equal to

$$\begin{aligned} \bar{F}(\omega,t_r) = &-\frac{|g|^2|\rho|^2\gamma(2\omega_p-\omega)^2\zeta_1(\omega,t_r)\zeta_1^*(\omega,t_r)}{\gamma(\omega)\gamma(2\omega_p-\omega)[4|g|^2|\eta|^2+\gamma(\omega)\gamma(2\omega_p-\omega)]-[\gamma(\omega)+\gamma(2\omega_p-\omega)]^2|g|^2|\rho|^2} \\ &+\frac{|g|^2|\rho|^2[\gamma(\omega)\gamma(2\omega_p-\omega)+\gamma(2\omega_p-\omega)^2]\big[\zeta_2(\omega,t_r)\zeta_2^*(\omega,t_r)+e^{\frac{\gamma(\omega)+\gamma(2\omega_p-\omega)}{2}t}\big]}{\gamma(\omega)\gamma(2\omega_p-\omega)[4|g|^2|\eta|^2+\gamma(\omega)\gamma(2\omega_p-\omega)]-[\gamma(\omega)+\gamma(2\omega_p-\omega)]^2|g|^2|\rho|^2} \\ &-\frac{\gamma(\omega)\gamma(2\omega_p-\omega)|g\rho\zeta_1(\omega,t_r)+[2g\eta+\gamma(2\omega_p-\omega)]\zeta_2(\omega,t_r)|^2}{\gamma(\omega)\gamma(2\omega_p-\omega)[4|g|^2|\eta|^2+\gamma(\omega)\gamma(2\omega_p-\omega)]-[\gamma(\omega)+\gamma(2\omega_p-\omega)]^2|g|^2|\rho|^2}. \end{aligned} \tag{59}$$

The results in (58) and (59) are extending the analytic solutions from [53] (when expressed in terms of complex exponentials). In contrast to the original work, our solution also includes a nonzero phase mismatch as well as chromatic dispersion in the time domain.

A. Gain and resonant phase matching

From (58), we obtain the well-known gain spectrum for a JTWPA [32,35] with additional exponential damping due to the inclusion of substrate losses. The gain G is given by the factor in front of the initial signal photon number $N_{s,0}$ at $t_r = 0$, i.e.,

$$G = \zeta_1(\omega, t_r)\zeta_1^*(\omega, t_r)e^{-\frac{\gamma(\omega)+\gamma(2\omega_p-\omega)}{2}t_r}. \tag{60}$$

Apart from the power gain spectrum in (60), which is determined by the parametric amplification of the signal photon field including substrate losses [35], one can define a quantum gain of a JTWPA as the ratio of the expected photon number at the output to the input photon number, which is given by

$$G_q = \frac{N_{\omega,t_r}}{N_{\omega,0}}. \tag{61}$$

In the classical limit, i.e., for a large number of input photons $N_{\omega,0}$ compared to the idler field and additional noise, the converted idler photons and thermal fluctuations can be neglected and we recover the power signal gain, as defined in (60).

It is crucial to minimize the frequency-dependent total phase mismatch $\Delta\Omega$ in order to achieve a high parametric gain over a large bandwidth. From (41), it is clear that the total phase mismatch $\Delta\Omega$ is affected by self- and cross-phase-modulation effects, as well as chromatic dispersion [32]. Thus, proper dispersion engineering by including resonant phase matchers [20] or spatial modulations of the transmission line structure [21] can have a huge impact on the overall amplifier performance. Resonant phase shifters, as depicted in blue (dark gray) color in Fig. 1, can be incorporated into our model by adjusting the dispersion relation accordingly. This is done by replacing the ground capacitance $C'\Delta z$ by a frequency-dependent impedance $Z(\omega)$ [31] in each unit cell:

$$Z(\omega) = \left[i\omega C'\Delta z + \frac{i\omega C_c(1 - L_r C_r \omega^2)}{1 - (C_r + C_c)L_r\omega^2}\right]^{-1}. \tag{62}$$

We still use the same reference timeframe $t = t_r$ from Sec. IV where, however, the dispersion factor $\Lambda_{RPM}(\omega)$ has to be adjusted according to

$$\frac{\partial t_{RPM}(\omega)}{\partial t_r} = \sqrt{\Lambda_{RPM}(\omega)} = \sqrt{\frac{\Lambda(\omega)}{i\omega Z(\omega)C'\Delta z}}. \tag{63}$$

B. Treatment of losses

In microwave engineering, substrate losses are typically expressed in terms of a loss tangent, which is defined as the ratio of the total effective conductivity to the lossless permittivity of the substrate [54]:

$$\tan\delta = \frac{\omega\varepsilon'' + \sigma}{\omega\varepsilon'}, \tag{64}$$

where ω is the angular frequency, σ is the conductivity per unit length, and $\varepsilon = \varepsilon' + i\varepsilon''$ is the permittivity of the substrate. Assuming that all internal losses are homogeneously distributed and only attributed to the substrate, the linear attenuation factor α can be calculated from the lossless propagation constant k_0 by

$$\alpha = \frac{k_0 \tan\delta}{2}. \tag{65}$$

Note that this simple linear loss model does not take into account additional losses due to, e.g., periodic loadings along the line, or pump saturation effects, which can however be included in a more elaborate approach for finding the respective coupling parameters $\gamma(\omega)$. The corresponding exponential damping factor $\tilde{\Gamma}(\omega)$ of a lossy JTWPA can hence be expressed as a function of the loss tangent:

$$\tilde{\Gamma}(\omega) = \frac{1}{2}\omega\sqrt{\frac{C'\Delta z}{L_{J,0}}}Z_0\tan\delta,$$

with the characteristic impedance Z_0 of the transmission line, where we have already switched the spatial description of the attenuation factor to a temporal description and taken into account the translation between the reference travel time t_r and the frequency-dependent propagation time $t(\omega)$. The classical damping factor $\tilde{\Gamma}(\omega)$ can then be related to the quantum-mechanical damping coefficients $\gamma(\omega)$ of our model by $2\tilde{\Gamma}(\omega) \mapsto \gamma(\omega)$.

TABLE I. JTWPA device parameters from [20,32]

Parameter	Symbol	Value
Josephson capacitance	C_J	329 fF
Josephson-junction critical current	I_c	3.29 μA
Pump current amplitude	I_p	$0.5I_c$
RPM coupling capacitance	C_c	10 fF
RPM resonator capacitance	C_r	7.036 pF
RPM resonator inductance	L_r	100 pH
Substrate loss tangent	$\tan\delta$	0.0025
Unit-cell ground capacitance	C	39 fF
Unit-cell number	N_{cell}	2000
Unit-cell physical length	l_{cell}	10 μm

C. Modeling of JTWPAs

We solved (58) and (61) for a well-studied structure from the literature [20,32] and used the result to demonstrate the parametric gain for a large number of input photons [see (60)]. The device parameters of the JTWPA are given in Table I.

In Fig. 2 the signal gain is given as a function of frequency. We have included both cases with and without resonant phase matching according to [20]. The literature results [20,32] for an ideal substrate could be reproduced by our model and are given in the gray (uppermost) and light gray (second-lowest) line in Fig. 2. The resulting gain considering a more realistic substrate material with a loss tangent of 0.0025 is given in

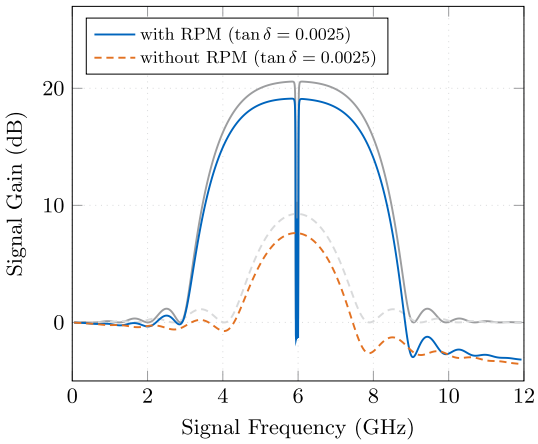

FIG. 2. Gain spectrum of a Josephson traveling-wave parametric amplifier including substrate losses with a loss tangent $\tan\delta = 0.0025$. The parameters of the JTWPA structure are taken from the literature [20,32] and are explicitly given in Table I. The blue (dark gray) line describes the gain spectrum with resonant phase matchers placed in every unit cell, while the dashed orange (dark gray) curve represents the signal gain without dispersion engineering. The upper gray lines represent the gain spectra for the lossless case with (upper solid) and without (upper dashed) phase matching, respectively.

solid blue (dark gray) and dashed orange (gray) color, for the case with and without resonant phase matching, respectively.

It can be seen that proper dispersion engineering can substantially enhance the device's performance in terms of gain and bandwidth, as pointed out in [20]. This becomes even more clear when taking a look at the temporal dynamics of the expected photon number in the signal mode. Assuming a single signal photon at the input of the JTWPA, the temporal evolution of the signal photon number is depicted in Fig. 3.

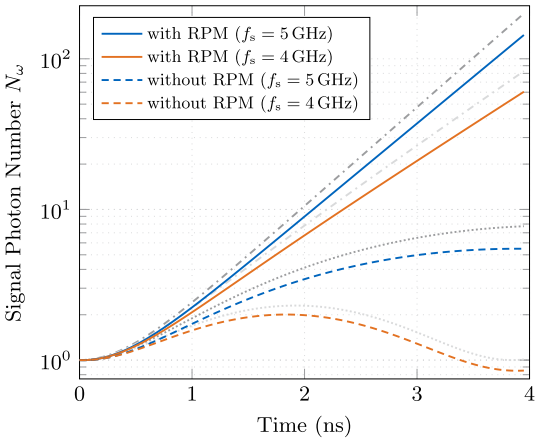

FIG. 3. Temporal evolution of the number of signal photons within the JTWPA from Table I. The blue (dark gray) lines describe the temporal dynamics of a signal mode with a center frequency of 5 GHz with (solid) and without (dashed) RPM. The orange (gray) curves represent the time evolution of a signal at 4 GHz, also with (solid) and without (dashed) RPM. The dash-dotted gray lines represent the temporal evolution for the lossless case at both frequencies, while the dotted lines correspond to the case without phase matching.

TABLE II. JTWPA device parameters from [36].

Parameter	Symbol	Value
Josephson plasma frequency	ω_J	$2\pi \times 46.5$ GHz
Josephson-junction critical current	I_c	4.4 μA
Pump current amplitude	I_p	$0.53 I_c$
Substrate loss tangent	$\tan\delta$	0.0025
Unit-cell ground capacitance	C	115 fF
Unit-cell inductance (unpumped)	L	312 pH
Unit-cell number	N_{cell}	1016
Unit-cell physical length	l_{cell}	26 μm

The time argument on the abscissa is given in terms of the reference timeframe from Sec. IV. The signal photon number at around 4 ns corresponds to the output of the amplifier after 2000 unit cells. With proper dispersion engineering, exponential gain can be achieved as it can be seen from the solid blue (upper) and solid orange (lower) curves in Fig. 3, corresponding to signal frequencies of 5 and 4 GHz, respectively. According to the gain spectrum in Fig. 2, a parametric gain of ≈15 dB can be achieved for a mode at 4 GHz with RPM. Without RPM, however, the gain attains a local minimum at 4 GHz and even becomes negative when dielectric losses are taken into account. The temporal dynamics in Fig. 3 reveal that without RPM, the signal mode at 4 GHz first experiences some gain until around 1.75 ns. From there on, the signal mode gets depopulated due to the large phase mismatch of the signal and pump modes, which results in an average photon number smaller than 1 at the output due to the transmission line losses. At 5 GHz, however, there is still some gain of around 5 dB, even without RPM.

The device parameters from [20,32] have so far only been studied theoretically. We now want to assess how our model performs for an experimentally realized structure, that has been reported in [36,55]. Equations (58) and (60) are used to predict the power gain of the signal mode, with the nonlinear transmission line parameters from [36]. The respective device parameters are summarized in Table II. We then compare our analytic results with the measured gain spectrum from [36] and demonstrate that our model is suitable as a design tool for predicting the device performance of realistic JTWPAs. In this particular device, no dispersion engineering was employed. Thus, the provided results comprise a relatively large phase mismatch compared to the previous resonantly phase-matched device, albeit not as large as for the case without RPM in [20,32]. The resulting gain spectrum with the parameters from Table II is given in terms of the blue (dark gray) curve in Fig. 4. The noisy light gray line was extracted from [36] and represents the experimentally determined gain spectrum. Comparing both curves shows good agreement of the predicted and measured spectra. An even better agreement was achieved by slightly modifying the device parameters. To account for pump depletion, we slightly decreased the pump current, assumed to be constant in our model, from $0.53 I_c$ to $0.51 I_c$. At the same time, we increased the unit-cell ground capacitance C from 115 to 140 fF. This results in an almost perfect match over the entire frequency range that was covered in the experiment (see the dashed curve in Fig. 4). The

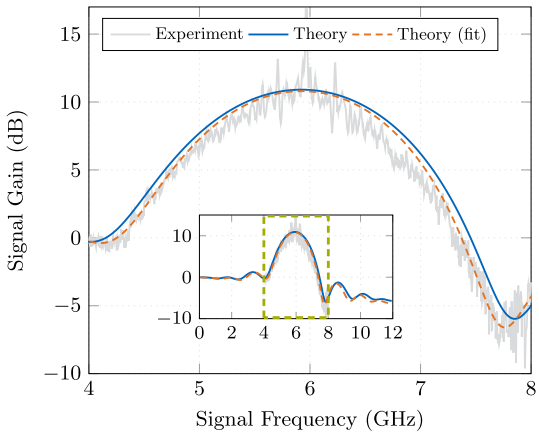

FIG. 4. Gain spectrum of the experimental JTWPA from [36] from 4 to 8 GHz. The respective parameters for the JTWPA unit cell are given in Table II. The noisy gray line in the background shows the measurement results for the JTWPA, extracted from Fig. 3 of [36]. The solid blue line depicts the resulting gain spectrum of our model using exactly the parameters given in Table II. A better fit (dashed orange line) to the experimental data was achieved by slightly increasing the unit-cell capacitance to 140 fF while decreasing the pump current to $0.51I_c$ to account for the neglected pump depletion. The inset shows the gain spectrum for the full 0–12-GHz frequency range.

inset plot shows the full spectrum as predicted by the analytic model, where the dashed green rectangle marks the frequency range where experimental data were available.

IX. ADDED NOISE ANALYSIS

Quantitatively, the noise figure of conventional low-noise amplifiers is due to the resistive nature of the amplification mechanism. Superconducting parametric amplifiers, in contrast, rely on nonlinear wave-mixing processes, where the added noise is not limited by dissipation [40]. Hence, the noise performance of a JTWPA is only restricted by quantum-mechanical limits on the fluctuations of the signals involved in the wave-mixing process [56]. The noise at the output of a linear amplifier can be separated into contributions of the amplified input fluctuations, and the noise added by the amplifier's internal degrees of freedom. The quantum noise is bounded by the uncertainty principle and gives rise to a standard quantum limit (SQL). In the following, we investigate the added noise of JTWPAs including substrate losses and associated fluctuations, and compare the predictions of our theory to experimental results.

Fluctuations within a quantum limited amplifier are usually evaluated based on the average of the field variance [56]. The quantum limit can then be given by a single added noise number A, defined as the number of energy quanta added to the input of a perfectly noiseless linear amplifier [4,57]. In the literature [35,52,58], this approach has been applied to study the effect of loss asymmetries as well as thermal and quantum noise in traveling-wave parametric amplifiers. According to [4], at this point, a distinction needs to be made in terms of the actual input and output signals. In our case, we consider a weak photon field at frequency ω with a narrow bandwidth $B_s \ll \omega$, which carries the information. This signal mode gets amplified by four-wave mixing while traveling along the Josephson-junction-embedded nonlinear transmission line, experiencing parametric gain, substrate losses, and noise added by the wave-mixing and the environmental fluctuations. The mean-square fluctuations $|\Delta\hat{A}_\omega|^2$ within the narrow bandwidth B_s of the annihilation operator $\hat{A}_\omega$ of the weak photon field are given by the symmetric variance:

$$\left|\Delta\hat{A}_{\omega,t_r}\right|^2 = \int_{\omega-\frac{B_s}{2}}^{\omega+\frac{B_s}{2}} \frac{1}{2}\langle \hat{A}_{\omega,t_r}\hat{A}^\dagger_{\omega',t_r} + \hat{A}^\dagger_{\omega,t_r}\hat{A}_{\omega',t_r}\rangle d\omega', \tag{66}$$

assuming vanishing expectation values $\langle\hat{A}_{\omega,t_r}\rangle$ and $\langle\hat{A}^\dagger_{\omega,t_r}\rangle$, which is the case for thermal and number states [42]. Using the Bosonic commutator relation $[\hat{A}_{\omega,t_r}, \hat{A}^\dagger_{\omega',t_r}] = \delta(\omega-\omega')$, it holds that after a reference interaction time t_r, the output fluctuations are equal to

$$\left|\Delta\hat{A}_{\omega,t_r}\right|^2 = \int_{\omega-\frac{B_s}{2}}^{\omega+\frac{B_s}{2}} \langle\hat{A}^\dagger_\omega\hat{A}_{\omega'}\rangle d\omega' + \frac{1}{2} = N_{s,t_r} + \frac{1}{2}. \tag{67}$$

Similarly, the mean-square fluctuations of the weak photon field at the input of the amplifier are given by $|\Delta\hat{A}_{\omega,0}|^2 = N_{s,0} + 1/2$. The mean-square fluctuations at the input and output of the amplifier are given in terms of energy quanta. Hence, when propagating through the device, the input fluctuations experience gain, while the inner degrees of freedom within the JTWPA add additional noise quanta [4]. This is reflected by the simple linear gain model

$$\begin{aligned}\left|\Delta\hat{A}_{\omega,t_r}\right|^2 &= G|\Delta\hat{A}_{\omega,0}|^2 + |\Delta\hat{\mathcal{F}}|^2_{op} \\ &= G\left[|\Delta\hat{A}_{\omega,0}|^2 + \frac{|\Delta\hat{\mathcal{F}}|^2_{op}}{G}\right],\end{aligned} \tag{68}$$

where $|\Delta\hat{\mathcal{F}}|^2_{op}$ represents the noise due to the inner degrees of freedom of the amplifier, borrowing the notation from [4]. The added noise A, i.e., the energy quanta added to the input due to the intrinsic quantum fluctuations of the amplifier, is then given by $A = |\Delta\hat{\mathcal{F}}|^2_{op}/G$. Thus, we can calculate the added noise A, given the expressions for the input and output fluctuations, i.e.,

$$A = \frac{\left|\Delta\hat{A}_{\omega,t_r}\right|^2}{G} - |\Delta\hat{A}_{\omega,0}|^2 = \frac{N_{s,t_r}+\frac{1}{2}}{G} - N_{s,0} - \frac{1}{2}. \tag{69}$$

Finally, it remains to determine an expression for the gain G, that is experienced by the input fluctuations in order to get the fluctuations at the output. From (68), we see that the gain G is given by the multiplicative factor in front of the input fluctuations $|\Delta\hat{A}_{\omega,0}|^2 = N_{s,0} + 1/2$ in the expression of the output mean-square fluctuations $|\Delta\hat{A}_{\omega,t_r}|^2 = N_{s,t_r} + 1/2$. By rearranging (58), it can be seen that $G = \zeta_1(\omega,t_r)\zeta_1^*(\omega,t_r)\exp\{-[\gamma(\omega)+\gamma(2\omega_p-\omega)]t_r/2\}$, which is exactly equal to the signal power gain in (60), as expected. Inserting the analytic solution for N_{s,t_r} from (58) and the expression for the power gain G from (60) into (69) yields the overall added noise of the parametric amplifier with substrate

loss, which is given by

$$A = \left[\bar{n}(\omega) + \frac{1}{2}\right]\left[\frac{1}{\zeta_1(\omega,t_\mathrm{r})\zeta_1^*(\omega,t_\mathrm{r})e^{-\frac{\gamma(\omega)+\gamma(2\omega_\mathrm{p}-\omega)}{2}t_\mathrm{r}}} - 1\right] + C_{\mathrm{si},0}\frac{\zeta_2^*(\omega,t_\mathrm{r})}{\zeta_1^*(\omega,t_\mathrm{r})} + C_{\mathrm{si},0}^*\frac{\zeta_2(\omega,t_\mathrm{r})}{\zeta_1(\omega,t_\mathrm{r})}$$
$$+ [N_{\mathrm{i},0} + \bar{n}(\omega) + 1]\frac{\zeta_2(\omega,t_\mathrm{r})\zeta_2^*(\omega,t_\mathrm{r})}{\zeta_1(\omega,t_\mathrm{r})\zeta_1^*(\omega,t_\mathrm{r})} + \left[\bar{n}(\omega) + \bar{n}(2\omega_\mathrm{p}-\omega) + 1\right]\frac{\bar{F}(\omega,t_\mathrm{r})}{\zeta_1(\omega,t_\mathrm{r})\zeta_1^*(\omega,t_\mathrm{r})}. \quad (70)$$

The first term in the second line of (70) gives the noise contributions due to the wave-mixing process with the fluctuations of the idler mode. The last term represents fluctuations due to thermal noise from the substrate interactions, which is particularly sensitive to the bath temperature. A lower bound on the added noise A for phase-insensitive linear amplifiers was derived and proven in [4], which is given by

$$A \geqslant \frac{1}{2}\left|1 - \frac{1}{G}\right|, \quad \text{for } G \geqslant 1. \quad (71)$$

Thus, in the high-gain limit $G \to \infty$ we obtain the half-photon SQL $\lim_{G\to\infty} A = 1/2$, which should be a reasonable limit within the spectral regions where one finally wants to operate a JTWPA. As a sanity check for our model, we investigated the lossless case where $T \to 0$ and $\gamma \to 0$. If we then let $G = |\zeta_1(\omega,t_\mathrm{r})|^2 \to \infty$, one can easily see that (70) also arrives at the SQL. In Sec. VII, we solved for the gain spectra of two parameter sets of different JTWPAs from the literature. In the following, we present our results on the added noise for both parameter sets, which are computed by solving (70). Let us first investigate the added noise of the JTWPA from [20,32], with the parameters summarized in Table I. For this particular parameter set, we assume a bath temperature $T = 50\,\mathrm{mK}$. In Fig. 5, the added noise is given as a function of frequency. The thick dashed orange (gray) line represents the added noise of the JTWPA without dispersion engineering. The thin dashed orange (gray) line depicts the gain spectrum for this case. The light gray (lowest) line represents the minimum added noise for the poorly phase-matched case. One can clearly see from the thick solid blue (dark gray) curve, which depicts the added noise over frequency including RPM, that proper dispersion engineering not only increases gain and bandwidth, but also considerably reduces the equivalent added noise at the input of the amplifier to around 0.55 quanta on average, just slightly above the quantum limit, given in solid dark gray color. The gain for the resonantly phase-matched case is given by the thin solid blue line. The gray shaded region is the forbidden area for the added noise in the dispersion engineered case, as the added noise cannot become negative, which is due to the fact that the gain must be larger than or equal to 1 for the limit in (71). If chromatic dispersion is properly compensated for, the quantum limit is close to the SQL, as the gain becomes relatively large, which is apparent from the inset in Fig. 5, which shows a zoom-in of the usable bandwidth of the amplifier. This device, as mentioned before, has however only been studied theoretically in [20,32]. In order to show the value and validity of our analytic model including losses and associated noise, we now have a closer look at the added noise of the experimentally studied JTWPA device from [36,55].

Evaluating (70) with the parameter set given in Table II yields the results depicted in Fig. 6. The associated experiments have been carried out at a temperature of $T = 20\,\mathrm{mK}$, which we also used for our modeling. In Sec. VII, we introduced a modified parameter set with slight variations on the line capacitance and the critical current in order to get a better fit for the gain spectrum to the experimental results. Thus, we also depict both results in Fig. 6, where the solid blue (dark gray) lines correspond to the added noise (thick) and gain spectrum (thin) for the original parameter set given in Table II, and the orange (gray) dashed lines represent the added noise and gain spectrum for the modified parameters. Also here, we show the minimum added noise according to (71) in the two lowest thick light and dark gray lines for the original and modified parameter sets, respectively. It shall be noted here that the modified parameter set was introduced for better matching of the modeled amplifier gain to the measured gain spectrum from [36]. However, we do not make any statement on better or worse matching for the added input noise, where the modified parameter set is just included for the sake of completeness. Compared to the previous device from [20], one can see that the added noise is somewhat higher, in the

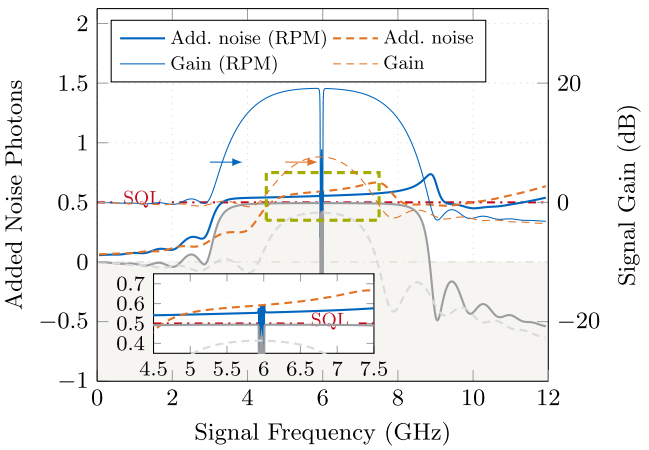

FIG. 5. Added noise of the JTWPA from [20,32] including substrate losses with a loss tangent $\tan\delta = 0.0025$ at $T = 50\,\mathrm{mK}$. The thick blue (dark gray) line describes the added noise with resonant phase matchers placed in every unit cell, while the thick dashed orange (gray) curve represents the added noise without dispersion engineering. The two lowest gray lines represent the limits on the added noise, with (solid) and without (dashed) phase matching. Additionally, the gain spectrum is given by the thin solid blue (dark gray) and thin dashed orange (gray) line for both cases (right axis). The inset shows a zoom-in of the added noise in the spectral range with a large gain. The gray shaded area at the bottom marks the forbidden range for the case with RPM.

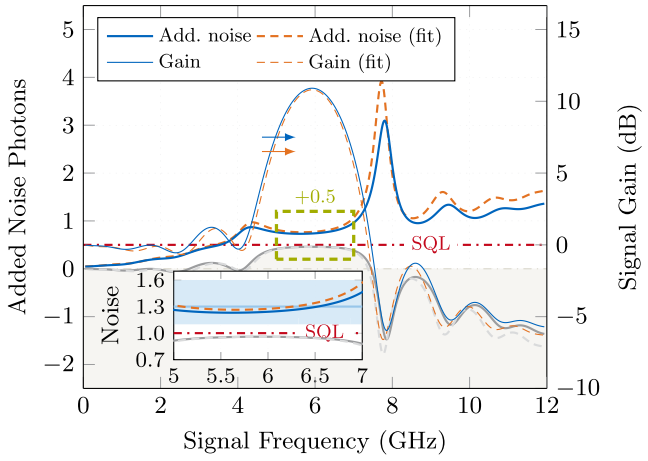

FIG. 6. Added noise of the experimental JTWPA from [36] for a temperature $T = 20\,\mathrm{mK}$. The thick solid blue (dark gray) line depicts the added noise calculated with our model using exactly the parameters given in Table II. The thick solid orange (gray) line corresponds to the modified parameter set (see Fig. 4). The two lowest gray lines mark the minimum added noise for the original (solid) and modified (dashed) parameter sets, respectively. The filled area in gray color represents the forbidden area. Additionally, the respective gain spectra are given by the thin solid blue (dark gray) and thin dashed orange (gray) lines. The inset shows the total equivalent noise at the input of the JTWPA in the usable spectral range within the highlighted green area. Excellent matching with the experimentally determined input noise of $1.3^{+0.3}_{-0.2}$ (light blue line and shaded area) from [36] is obtained.

range of around 0.8 quanta on average. In the experiment in [36], the noise temperature at the input of an amplifier cascade including the JTWPA was measured with the so-called Y-factor method [54]. The intrinsic noise of the JTWPA was then calculated by subtracting different signal paths, one that included the JTWPA and one that was short-circuited. The noise temperature translates into the total variance at the input of the amplifier, including the half quantum in (67) for $t_\mathrm{r} = 0$. Thus, in the inset in Fig. 6, we added this half quantum to be able to compare the resulting input fluctuations with the experimental results of $1.3^{+0.3}_{-0.2}$. The experimental input photon variance is given as a solid light blue (light gray) line, with the uncertainty range highlighted as a light blue (light gray) area. The predictions of our theory on the added input fluctuations are precisely within the uncertainty of the experimental observation, as apparent from the inset of Fig. 6. Actually, the added noise for both parameter sets, original and modified, is within the experimental measurement uncertainty over the entire usable bandwidth.

X. CONCLUSION

In this paper, we introduced a rather complete quantum circuit model for a Josephson traveling-wave parametric amplifier operating in the four-wave-mixing mode, including self- and cross-phase modulation, phase mismatching due to chromatic dispersion, as well as losses and associated fluctuations due to the imperfect substrate isolation. In contrast to existing literature [20,21,31,35] where the amplification is investigated over the interaction length in terms of a spatial description, we presented the temporal evolution of the mode operators based on the Heisenberg equations in the scattering limit (i.e., assuming perfect impedance matching). An attempt for such a temporal formulation was given in [32], however, without proper accounting for dispersion. We included dispersion by introducing a reference timeframe with associated dispersion factors in the respective signal and idler modes. From the system and bath dynamics, we formulated coupled mode temporal evolution equations for the creation and annihilation operators of the weak idler and signal photon fields. Even for the general case, including nonzero dispersion and phase matching as well as substrate losses and associated fluctuations, we found an analytic solution for the signal annihilation operator, assuming a strong classical monochromatic pump tone. Losses are here included by means of a loss tangent that is associated with the bath interaction strength. Using this analytic solution, we found an expression for the temporal evolution of the photon number in the signal mode. Based on this, we were able to predict the gain spectrum of the amplifier, which was validated against results from the literature for the lossless case. A direct comparison of the gain spectrum predicted by our model to results of an experimental device yielded very good agreement over the full frequency range. Finally we derived and evaluated the noise added to the input variance of JTWPAs. Also here, our predictions were found to be in excellent agreement with measured results from the literature.

ACKNOWLEDGMENT

The research is part of the Munich Quantum Valley, which is supported by the Bavarian state government with funds from the Hightech Agenda Bayern Plus.

[1] J. B. Johnson, Phys. Rev. **32**, 97 (1928).
[2] H. Nyquist, Phys. Rev. **32**, 110 (1928).
[3] B. Abdo, F. Schackert, M. Hatridge, C. Rigetti, and M. Devoret, Appl. Phys. Lett. **99**, 162506 (2011).
[4] C. M. Caves, Phys. Rev. D **26**, 1817 (1982).
[5] M. D. Reed, L. DiCarlo, B. R. Johnson, L. Sun, D. I. Schuster, L. Frunzio, and R. J. Schoelkopf, Phys. Rev. Lett. **105**, 173601 (2010).
[6] A. A. Clerk, M. H. Devoret, S. M. Girvin, F. Marquardt, and R. J. Schoelkopf, Rev. Mod. Phys. **82**, 1155 (2010).
[7] B. D. Josephson, Phys. Lett. **1**, 251 (1962).
[8] G. Johansson, L. Tornberg, V. S. Shumeiko, and G. Wendin, J. Phys.: Condens. Matter **18**, S901 (2006).
[9] G. Wendin and V. S. Shumeiko, Low Temp. Phys. **33**, 724 (2007).
[10] F. Mallet, F. R. Ong, A. Palacios-Laloy, F. Nguyen, P. Bertet, D. Vion, and D. Esteve, Nat. Phys. **5**, 791 (2009).
[11] H. Zimmer, Appl. Phys. Lett. **10**, 193 (1967).
[12] P. Russer, Arch. Elektr. Übertr. **23**, 417 (1969).
[13] P. Russer, Proc. IEEE **59**, 282 (1971).

[14] P. Russer and J. A. Russer, IEEE Trans. Microw. Theory Techn. **59**, 2685 (2011).

[15] X. Gu, A. F. Kockum, A. Miranowicz, Y.-X. Liu, and F. Nori, Phys. Rep. **718-719**, 1 (2017).

[16] J. Y. Mutus, T. C. White, R. Barends, Y. Chen, Z. Chen, B. Chiaro, A. Dunsworth, E. Jeffrey, J. Kelly, A. Megrant, C. Neill, P. J. J. O'Malley, P. Roushan, D. Sank, A. Vainsencher, J. Wenner, K. M. Sundqvist, A. N. Cleland, and J. M. Martinis, Appl. Phys. Lett. **104**, 263513 (2014).

[17] C. Macklin, K. O'Brien, D. Hover, M. E. Schwartz, V. Bolkhovsky, X. Zhang, W. D. Oliver, and I. Siddiqi, Science **350**, 307 (2015).

[18] P. Russer, Wiss. Ber. AEG-Telefunken **50**, 171 (1977).

[19] P. Russer, Circuit arrangement for amplifying high frequency electromagnetic waves, US Patent No. 4,132,956 (1979)

[20] K. O'Brien, C. Macklin, I. Siddiqi, and X. Zhang, Phys. Rev. Lett. **113**, 157001 (2014).

[21] L. Planat, A. Ranadive, R. Dassonneville, J. Puertas Martinez, S. Léger, C. Naud, O. Buisson, W. Hasch-Guichard, D. M. Basko, and N. Roch, Phys. Rev. X **10**, 021021 (2020).

[22] A. Ranadive, M. Esposito, L. Planat, E. Bonet, C. Naud, O. Buisson, W. Guichard, and N. Roch, Nat. Commun. **13**, 1737 (2022).

[23] O. Yaakobi, L. Friedland, C. Macklin, and I. Siddiqi, Phys. Rev. B **87**, 144301 (2013).

[24] H. A. Haus, Proc. IEEE **58**, 1599 (1970).

[25] B. Yurke and J. S. Denker, Phys. Rev. A **29**, 1419 (1984).

[26] H. A. Haus and Y. Yamamoto, IEEE J. Quantum Electron. **23**, 212 (1987).

[27] U. Vool and M. Devoret, Int. J. Circ. Theor. Appl. **45**, 897 (2017).

[28] F. X. Kaertner and P. Russer, Phys. Rev. A **42**, 5601 (1990).

[29] A. D. Armour, B. Kubala, and J. Ankerhold, Phys. Rev. B **91**, 184508 (2015).

[30] W. Kaiser, M. Haider, J. A. Russer, P. Russer, and C. Jirauschek, Int. J. Circ. Theor. Appl. **45**, 864 (2017).

[31] A. L. Grimsmo and A. Blais, npj Quantum Inf. **3**, 20 (2017).

[32] T. H. A. van der Reep, Phys. Rev. A **99**, 063838 (2019).

[33] M. Sargent III, M. O. Scully, and W. E. J. Lamb, *Laser Physics*, 1st ed. (Addison-Wesley, Reading, MA, 1974).

[34] M. Haider, Y. Yuan, and C. Jirauschek, *International Applied Computational Electromagnetics Society Symposium (ACES) Hamilton, ON, Canada* (2021), pp. 1–4.

[35] M. Houde, L. C. G. Govia, and A. A. Clerk, Phys. Rev. Appl. **12**, 034054 (2019).

[36] S. Simbierowicz, V. Vesterinen, J. Milem, A. Lintunen, M. Oksanen, L. Roschier, L. Grönberg, J. Hassel, D. Gunnarsson, and R. E. Lake, Rev. Sci. Instrum. **92**, 034708 (2021).

[37] W. B. Davenport and W. L. Root, *An Introduction to the Theory of Random Signals and Noise* (Wiley, New York, 1987).

[38] R. H. Koch, D. J. Van Harlingen, and J. Clarke, Phys. Rev. Lett. **45**, 2132 (1980).

[39] A. Roy and M. Devoret, C. R. Phys. **17**, 740 (2016).

[40] R. Kubo, Rep. Prog. Phys. **29**, 255 (1966).

[41] P. Russer, *Electromagnetics, Microwave Circuit and Antenna Design for Communications Engineering*, 2nd ed. (Artech House, Boston, 2006).

[42] S. Barnett and P. M. Radmore, *Methods in Theoretical Quantum Optics* (Clarendon, Oxford, 1997).

[43] N. Quesada and J. E. Sipe, Phys. Rev. A **90**, 063840 (2014).

[44] N. Quesada and J. E. Sipe, Phys. Rev. Lett. **114**, 093903 (2015).

[45] M. Liscidini, L. G. Helt, and J. E. Sipe, Phys. Rev. A **85**, 013833 (2012).

[46] A. B. Zorin, Phys. Rev. Appl. **6**, 034006 (2016).

[47] J. R. Zurita-Sánchez and C. Henkel, Phys. Rev. A **73**, 063825 (2006).

[48] C. Jirauschek and P. Russer, *Nonlinear Dynamics of Electronic Systems (NDES)* (Wolfenbuettel, Germany, 2012), pp. 1–4.

[49] V. Weisskopf and E. Wigner, Z. Phys. **65**, 18 (1930).

[50] K. Peng, M. Naghiloo, J. Wang, G. D. Cunningham, Y. Ye, and K. P. O'Brien, PRX Quantum **3**, 020306 (2022).

[51] A. B. Zorin, Phys. Rev. Appl. **12**, 044051 (2019).

[52] L. Fasolo, C. Barone, M. Borghesi, G. Carapella, A. P. Caricato, I. Carusotto, W. Chung, A. Cian, D. Di Gioacchino, E. Enrico, P. Falferi, M. Faverzani, E. Ferri, G. Filatrella, C. Gatti, A. Giachero, D. Giubertoni, A. Greco, C. Kutlu, A. Leo, C. Ligi, P. Livreri, G. Maccarrone, B. Margesin, G. Maruccio, A. Matlashov, C. Mauro, R. Mezzena, A. G. Monteduro, A. Nucciotti, L. Oberto, S. Pagano, V. Pierro, L. Piersanti, M. Rajteri, A. Rettaroli, S. Rizzato, Y. K. Semertzidis, S. Uchaikin, and A. Vinante, IEEE Trans. Appl. Supercond. **32**, 1700306 (2022).

[53] D. A. Holm and M. Sargent III, Phys. Rev. A **35**, 2150 (1987).

[54] D. M. Pozar, *Microwave Engineering*, 4th ed. (Wiley, New York, 2012).

[55] Leif Grönberg, M. Kiviranta, V. Vesterinen, J. Lehtinen, S. Simbierowicz, J. Luomahaara, M. Prunnila, and J. Hassel, Supercond. Sci. Technol. **30**, 125016 (2017).

[56] H. A. Haus and J. A. Mullen, Phys. Rev. **128**, 2407 (1962).

[57] C. M. Caves, J. Combes, Z. Jiang, and S. Pandey, Phys. Rev. A **86**, 063802 (2012).

[58] S. Zhao and S. Withington, J. Phys. D: Appl. Phys. **54**, 365303 (2021).